Becker, D., Meier, T., Bohnhoff, M., Harjes, H.-P. (2010): Seismicity at the convergent plate boundary offshore Crete, Greece, observed by an amphibian network. - Journal of Seismology, 14, 2, 369-392

DOI: 10.1007/s10950-009-9170-2

Seismicity at the convergent plate boundary offshore Crete, Greece, observed by an amphibian network

D. Becker[*], T. Meier[†], M. Bohnhoff[‡], H.-P. Harjes[†]

December 8, 2010

Abstract

We investigate microseismic activity at the convergent plate boundary of the Hellenic Subduction Zone (HSZ) on- and offshore south-eastern Crete with unprecedented precision using recordings from an amphibian seismic network. The network configuration consisted of up to eight ocean bottom seismometers (OBS) as well as five temporary short-period and six permanent broad-band stations on Crete and surrounding islands.

More than 2500 local and regional events with magnitudes up to $M_L = 4.5$ were recorded during the time period July 2003 - June 2004. The magnitude of completeness varies between 1.5 on Crete and adjacent areas and increases to 2.5 in the vicinity of the Strabo trench 100 km south of Crete. Tests with different localization schemes and velocity models showed that the best results were obtained from a probabilistic earthquake localization using a 1-D velocity model and corresponding station corrections obtained by simultaneous inversion.

Most of the seismic activity is located offshore of central and eastern Crete and interpreted to be associated with the intra-crustal graben system (Ptolemy and Pliny trenches). Furthermore, a significant portion of events represents interplate seismicity along the NNE-ward dipping plate interface. The concentration of seismicity along the Ptolemy and Pliny trenches extends from shallow depths down to the plate interface and indicates active movement. We propose that both trenches form transtensional structures within the Aegean plate. The Aegean

[*]Institute of Geophysics, Hamburg University, Bundesstr. 55, 20146 Hamburg, Germany
[†]Institute of Geology, Mineralogy and Geophysics, Ruhr University Bochum, Germany
[‡]GeoForschungsZentrum Potsdam, Potsdam, Germany

continental crust between these two trenches is interpreted as a forearc sliver as it exhibits only low microseismic activity during the observation period and little or no internal deformation. Interplate seismicity between the Aegean and African plates forms a 100 km wide zone along dip from the Strabo trench in the south to the southern shore-line of Crete in the north. The seismicity at the plate contact is randomly distributed and no indications for locked zones were observed. The plate contact below and north of Crete shows no microseismic activity and seems to be decoupled. The crustal seismicity of the Aegean plate in this area is generally confined to the upper 20 km in agreement with the idea of a ductile deformation of the lower crust caused by a rapid return flow of metamorphic rocks that spread out below the forearc. In the region of the Messara half-graben at the south coast of central Crete a southward dipping seismogenic structure is found that coalesces with the seismicity of the Ptolemy trench at a depth of about 20 km. The accretionary prism south of Crete indicated by the Mediterranean Ridge showed no seismic activity during the observation period and seems to be deforming aseismically.

1 Introduction

1.1 Tectonic setting of the Hellenic Subduction Zone

The Hellenic Subduction Zone, referred to as HSZ hereafter, is the seismically most active region in Europe. This high seismic activity is caused by the subduction of the oceanic African lithosphere beneath the continental Anatolian-Aegean lithosphere as manifested by Benioff zone seismicity (Papazachos and Comninakis, 1971; Makropoulos and Burton, 1984; Papazachos et al., 2000) and seen in the images of seismic tomography (Spakman et al., 1988; Spakman et al., 1993; Papazachos and Nolet, 1997). According to Thompson et al. (1998) the current active margin south of Crete was initiated approximately 15 Ma ago following earlier subduction of oceanic basins north of the present day active margin and accretion of continental terranes to Eurasia (Dercourt et al., 1986; Gealey, 1988). Neotectonic reconstructions indicate a migration of the active margin approximately 400-500 km to the south-west during the last 15 Ma (ten Veen and Meijer, 1998; ten Veen and Kleinspehn, 2003). The retreat of the active margin is caused by slab-pull of the downgoing African lithosphere (Angelier et al., 1982; LePichon et al., 1995; Laigle et al., 2004). In the same time interval, the

African plate approached Eurasia by about 150 km (Dercourt et al., 1986; Gealey, 1988; Facenna et al., 2003). At present the Aegean plate moves towards the south-west at 3.0-3.5 cm/yr with respect to stable Eurasia while the African plate exhibits a northward drift of less than 1 cm/yr within the same reference frame (McClusky et al., 2000).

The HSZ in the region of western Crete seems to enter the phase of continent-continent collision (Armijo et al. 1992; ten Veen and Kleinspehn, 2003) with the passive continental margin of Africa entering the subduction (Meier et al., 2004a). While subduction below western Crete occurs almost normal to the continental margin of the Aegean plate, subduction becomes more and more oblique towards the east (LePichon et al., 1995). Offshore central and eastern Crete the ongoing slab rollback in the Cretan-Rhodes section of the Aegean forearc is the likely cause for the transtensional structures within the continental Aegean lithosphere which are the dominating features south of central and eastern Crete (ten Veen and Kleinspehn, 2003). These structures are indicated in Fig. 1 by solid lines. In the vicinity of the Ptolemy and Pliny trenches wedge-shaped sedimentary basins were imaged from wide-aperture seismic profiles (Bohnhoff et al., 2001) and swath-mapping and seismic reflection profiles in the region of the Pliny and Strabo trenches show en echelon troughs and normal faulting (e.g. Huchon et al., 1982; LePichon et al., 1982; Huguen et al., 2001). Towards the west this graben system continues in the Ionian trench which is interpreted as an extensional structure within the Aegean lithosphere (Lallemant et al., 1994) that shows currently little microseismic activity (Meier et al., 2004b). All these so called trenches are interpreted as structures within the continental Aegean crust while the margin of the Aegean lithosphere is found further south buried below a thick sedimentary cover (Lallemant et al., 1994; Mascle et al., 1999; Huguen et al., 2001).

1.2 Seismicity of the HSZ

For the area of the HSZ an extensive historic catalogue (Papazachos et al., 2000), spanning the last 2500 years, as well as a number of microseismicity studies investigating the entire (Hatzfeld et al., 1993) or parts of the forearc (e.g. Delibasis et al., 1999; Becker, 2000; Meier et al., 2004b; Meier et al. 2007) are available in addition to global catalogues covering the second half of the 20th century (e.g. Engdahl et al., 1998).

Interplate seismicity in the HSZ follows the amphitheatrical shape of the Benioff zone from the Kefalonia fault in the west to the Turkish coast north-east of Rhodes in the east. Fig. 2 depicts this activity in the vicinity of Crete. Towards the north, the Benioff zone seismicity of the HSZ can be traced to depths of up to 180 km in the eastern part close to Rhodes and depths of approximately 100 km below Milos in the West using the relocated events of the ISC catalogue (Engdahl et al., 1998; Fig. 2) with much stronger activity in the central and eastern part than in the west.

According to the catalogue of historic earthquakes of the Aegean region compiled by Papazachos et al. (2000) the largest documented event with a magnitude of about $M_w 8.3$ (Papazachos et al., 2000; Stiros, 2001) occurred in 365 AD in the western forearc of the subduction zone south-west of Crete and it is suggested that this event caused the observed coastline uplifts of up to 9 m on western Crete and up to 2.5 m on the adjacent island of Antikythira (Pirazzoli, 1996; Stiros, 2001; Shaw et al., 2008). This event presumably ruptured the plate interface between the African and Aegean plates (Papazachos and Papazachou, 1997; Papazachos et al., 1999) on a lateral extent of 300 km from south of central Crete up to 22°E (Papazachos, 1996). However, the uplift could as well be explained by an event within the upper plate below Crete, a slow uplift over a longer time period or a series of small events (Shaw et al., 2008). The eastern portion of the plate interface in this region currently exhibits strong seismicity (Fig. 2).

In instrumental seismicity data (Engdahl et al., 1998) crustal seismicity within the upper plate is found in the central and eastern offshore region south of Crete in the vicinity of the Ptolemy trench and further south between the Pliny and Strabo trench. Some historic events are located in the same area (Papazachos et al., 2000) although it is generally not possible to discriminate between intra- and interplate activity for these events due to weakly constrained hypocentral depths. Remarkably, almost all of the shallow strong historic activity with magnitudes of $M_w \geq 6$ locates close to the Cretan shore in the area of the Ptolemy trench or even onshore while the medium sized instrumental activity which is generally in the range of $M_w 3.5 - 5$ is found in its majority further south between Pliny and Strabo. However, we cannot exclude that this difference is caused by poor hypocentre precision of the historic events. Most of this shallow activity is likely to be caused by relative movements along transtensional structures caused by the oblique subduction and slab roll-back (Kahle et al., 2000; ten Veen and Kleinspehn, 2003; Bohnhoff et al., 2005). In the western offshore area,

seismicity is generally confined to the plate interface with low seismic activity at the Ionian trench. Historic and instrumental data are in good agreement for this region. Seismic activity on Crete itself is generally lower and occurs predominantly on north-south striking normal faults in the west that are capable of producing events up to M_w 5.5 (de Chabalier et al., 1992) and a trend of increasing activity towards the east with some strong historic events along the south coast of central and eastern Crete. Towards the north in the Cretan Sea hardly any shallow seismic event is observed and most of the seismicity occurs at intermediate depth.

Microseismicity studies in the forearc of the HSZ complement the historic and instrumental data sets. Several microseismic studies were conducted on the islands of Crete and Gavdos with temporary short period networks to study the distribution of microseismic activity in the region. In 1988 a study of microseismic activity covering the whole southern Aegean Sea recorded only sparse microseismic activity onshore Crete while most activity occurred south of Crete between the Pliny trench and the coast (Hatzfeld et al., 1993). A study conducted in 1995 in central Crete (Delibasis et al., 1999), however, found significant microseismic activity in the Messara graben, the Heraklion Basin and in the southern offshore region at the Ptolemy trench. This latter activity was also observed during a 2000/2001 field campaign aimed at studying the microseismic activity in central Crete (Meier et al., 2004a). Field campaigns in the years 1996-2002 mapped microseismic activity at the plate interface (Meier et al., 2004a) and identified an offset between the southern border of the Aegean lithosphere and the southern border of active interplate seismicity. Most of the offshore activity in the western part originated at the plate contact with only little activity in the Ionian trench. A microseismic study in eastern Crete in early 1999 found abundant activity onshore eastern Crete as well as in the southern offshore region (Becker, 2000).

The only OBS network operated so far in the Libyan Sea consisted of five analogue OBS stations that were deployed southeast of Crete for 8 days in July 1988. 1000 microearthquakes were detected of which more than 140 were located (Kovachev et al., 1991; Kovachev et al., 1992). The authors interpreted the spatial distribution of the hypocentres as an en-echelon positioning of the subduction zone manifested bathymetrically in the Strabo and Pliny trenches.

The aim of this study is to better resolve the seismogenic regions in the area offshore central and eastern Crete. The study region includes the offshore graben system as well as the plate contact in that area and the accretionary prism to the south. The area

of investigation had not yet been analyzed for (micro)seismic activity using modern digital ocean bottom instrumentation combined with stations on Crete, allowing to decrease the magnitude-detection threshold to below M3.5. The inset of Fig. 2 shows a cross-section incorporating information from the global ISC catalogue and data from an onshore network (Becker, 2000). While the global data is to sparse to accurately define the seismogenic structures, the local network is restricted to events onshore and close to the Cretan shore. The installation of an amphibian network covering the entire trench system south of central and eastern Crete on the other hand should allow a precise localization of the seismogenic zones in this area by significantly improving the location accuracy of offshore events and reducing the detection threshold.
Furthermore, we aim at investigating the influence of different velocity models and localization techniques on the hypocentral distribution and location precision. Therefore, two different 1-D and a simple 3-D model are tested in conjunction with a gradient method and a probabilistic localization scheme for the determination of the hypocentral coordinates. The performance of the different localization methods is compared and the best constrained seismicity distribution is used to interpret the results with regard to the regional seismotectonic setting.

2 Experimental Setup and Data Processing

The initial station distribution of the amphibian network (LIBNET) aimed at monitoring the entire trench system SE of Crete as well as the supposed southern border of the Aegean plate. Therefore, one OBS (LIB1 in Fig. 2) was placed at a location presumably on top of the oceanic African lithosphere as suggested by refraction seismic studies (Brönner, 2003). With this station layout a lower detection threshold, a better location precision for crustal seismicity within the Aegean plate as well as better depth constraints for events at the plate boundary were expected compared to land based networks or networks of regional or global scale. Thus, the identification of active structures within the continental Aegean crust south of Crete as well as the determination of the updip limit of interplate seismicity becomes a realistic target. Furthermore, it permits a glimpse at the accretionary complex to the south with its mud volcanism (Fig. 1; Kopf, 2002).

The LIBNET campaign was carried out in five separate observation phases during which up to 8 OBS stations were deployed for a recording period of up to 60 days. After each deployment period the OBS were recovered and then redeployed. Except for one OBS in the last observation phase which was equipped with a CME-40 broad-band sensor all OBS stations were equipped with 3 short-period SM-6 B-coil geophones (one vertical and two horizontal components) with a natural frequency of 4.5 Hz. Data loggers were of the SEDIS type (www.geopro.com/instrumentation/sedis-v.html). The sampling rate was 128 Hz or 250 Hz, respectively and a clock drift correction was applied to the data after station recovery. A maximum of 6 stations produced reliable recordings within each recording period.

The onshore part of LIBNET consisted of five short-period stations equipped with Mark L4-3D seismometers and PDAS-100 data loggers operated at 50 Hz sampling frequency. In addition, permanent broad-band stations were incorporated in the data analysis equipped with either STS-2 Streckeisen seismometers or Lennartz LE-20/3D sensors. These stations are part of the GEOFON (Hanka & Kind, 1994), the National Observatory of Athens (NOA) and MEDNET networks, respectively. Data from these stations were provided by the GEOFON data centre in Potsdam, Germany (http://www.gfz-potsdam.de/geofon/).

Due to the inferior data quality of the southernmost OBS stations (Fig. 3a), presumably caused by the thick sedimentary cover and week coupling conditions, the last two deployment periods were carried out with a modified network geometry. Station coverage in the northern part of the study region was densified by deploying all OBS stations between the south coast of Crete and the Strabo trench (Fig. 2). This allowed to obtain higher data recovery rates for the last two deployment periods and to further lower the detection threshold for events in the seismically active offshore region between Crete and the Strabo trench.

During data processing, continuous waveforms from LIBNET stations and the temporary short period onshore stations were filtered between 2 and 20 Hz and a STA/LTA trigger (Robinson, 1967) was applied for event detection. The subsequent application of a coincidence trigger required a minimum of 3 stations triggering within 19 seconds. This time interval was chosen due to the inter-station distances and the assumption of low seismic velocities within the thick sedimentary cover.

High seismic activity was observed throughout the whole observation campaign with occasional bursts of activity consisting of more than 100 events per day. However, these

events were often small and only recorded at one or two stations and thus not included in the further data processing. The best data quality for OBS stations is found in the region between Crete and the Pliny trench while stations further south exhibited considerably lower signal to noise ratios (SNRs) and often very long signal coda (Fig. 3a). This variation in data quality might be explained by a thick, water saturated sediment cover present in the southern part which also prevented signal penetration during active seismic experiments in the region (Brönner, 2003). The few intra-slab events detected from below Crete and the Sea of Crete, on the other hand, exhibit high SNRs on the northernmost OBS stations (Fig. 3b) and indicate the waveguide quality of the subducting African slab.

The triggering procedure led to the identification of 3257 potential events covering the time period July 2003 - June 2004. After visual inspection and elimination of teleseismic and multiple triggered events a total of 2686 local and regional events were further analyzed. 17173 P- and 15995 S-phase onsets were picked manually on the vertical component for the P-phase and on the horizontal components for the S-phase. Local Richter magnitudes were calculated for the events from restituted displacement proportional records simulating the recording of a Wood-Anderson seismometer and taking into account a distance correction suggested for events in the Aegean (Kiratzi and Papazachos, 1984).

3 Event Localization Procedure

To achieve an optimal hypocentre determination and to investigate the influence of the localization scheme and the velocity model on the seismicity distribution, four different approaches were tested: (1) An initial velocity model derived in an earlier study (Meier et al., 2004a) in conjunction with a gradient method, (2) a minimum 1-D velocity model gained by simultaneous inversion for the velocity model and station corrections, (3) a simple 3-D velocity model used in conjunction with a probabilistic event localization technique and (4) a probabilistic event localization applied to the minimum 1-D velocity model with corresponding station corrections. With these tests the influence of the slab and the horizontally varying velocity structure on the seismicity distribution can be investigated. Furthermore, by the probabilistic approach the model space is more completely sampled and no termination of the location

procedure in local minima close to the initial event location occurs.

3.1 Initial Event Localization

Initial event locations were obtained using the hypoinverse2000 location software (Klein, 2002) and a velocity model obtained during earlier seismological and seismic studies in the region (Bohnhoff et al., 2001; Brönner, 2003; Meier et al., 2004a; Fig. 4a). This velocity model is very similar to the one derived by Meier et al. (2004a) in a microseismicity study for the region of central Crete which was obtained by solving for a minimum 1-D model using the VELEST inversion software (Kissling et al., 1994). A v_p/v_s velocity ratio of 1.78 was adopted after evaluation of Wadati plots for events within the network. Because hypoinverse2000 assumes all stations to be at zero elevation station delays were estimated for OBS as well as onshore stations according to their respective elevation above or below the top of the velocity model. The starting depth was varied between 5 and 150 km and the hypocentre calculation was terminated after 40 iterations. The solution with the smallest rms value and location uncertainty was adopted as hypocentre. The step size of the starting depth variation was 5 km down to 40 km depth and increasingly larger below. This approach was chosen to more completely sample the depth space and avoid termination of the localization program in a local minimum. This significantly increased the number of events converging to a low rms solution within the given number of iterations when compared to a single location run with just one fixed starting depth.

3.2 Joint Determination of Hypocentres and 1-D Velocity Model

To obtain a more realistic 1-D velocity model for the entire study region and station corrections that account for site specific velocity anomalies, a simultaneous inversion using the VELEST software was performed.
The inversion scheme simultaneously solves for velocity model and station corrections by a least squares formulation minimizing the weighted misfit between predicted and observed arrival times. Details and limitations of this inversion procedure were given by Kissling et al. (1994). This results in a minimum 1-D velocity model with

corresponding station corrections and hypocentre locations. Inversion for the minimum 1-D velocity model was performed using version 3.3 of the VELEST software. As input, 435 events from the initial hypoinverse2000 localization (see Fig. 5d) with at least 6 P readings, an azimuthal gap less than 180 degrees, an rms value of less than 0.7 s and horizontal and vertical errors less than 10 and 15 kilometers, respectively, as indicated by the hypoinverse2000 routine, were used. Onshore station CCD served as reference station. This station exhibits an almost continuous data record for the whole observation period and high data quality. The more than 100 starting models which sample a wide range of the model space and contain no low velocity zones for stability reasons are depicted in Fig. 5a. During the inversion hypocentre and station files were updated after each VELEST run and after 5 VELEST runs all available events were relocated and those satisfying the above mentioned criteria were reselected for the next iteration of the inversion. The number of finally selected events for the different inversion runs covers the range from 301 up to 513 selected events with 85 of the velocity models being constrained by more than 450 events. This reflects the fact that most of the models obtained by inversion are slower than the initial model used for localization. Models constrained by only slightly more than 300 events have very high velocities which results in the exclusion of many events locating now outside the network and having an azimuthal gap of more than 180 degrees. These models also have very high average rms values and thus show a worse fit to the data than the models with lower velocities which are constrained by more events. Figs. 5a,b show the resultant velocity models colour-coded according to the model misfit. The velocity model is best constrained between 15 and 35 km depth where the P-velocity is of the order of 6 km/s. Due to the distribution of the recording stations and the hypocentres the ray density in this depth range is very high which allows a good determination of the layer velocities. This can be seen from Fig. 5a were the 10 velocity models with the best rms fit are plotted above the initial velocity models and only exhibit a small scatter in this depth range. For depths below 35 km the event density starts to decrease, resulting in less ray paths constraining the model because most recorded onsets are direct waves and not refractions. However, a gradual stepwise increase of the velocity is observed for nearly all models for depths below 35 km reaching values of 7.5-7.9 km/s at 50 km depth for models with the smallest rms misfit (Fig. 5a). At shallower depths the velocity models with the smallest rms misfits indicate P-velocities of $\leq 4.5\,km/s$. The lack of convergence for velocity models within the uppermost

10 km might be explained with the strong lateral velocity variations in that depth range. Because there was no single preferable velocity model, the arithmetic mean of the 10 models with the lowest rms was adopted as minimum 1-D velocity model (Fig. 4b). Station corrections for this minimum 1-D velocity model were obtained by a final VELEST inversion run. The initial 435 events used in the inversion were taken as input for this run. A constant v_p/v_s ratio of 1.78 was assumed and the P-velocities were fixed to those of the minimum 1-D velocity model by overdamping. Calculated station corrections (Fig. 5d) show increasingly positive values towards the south-east while values for stations close to the south coast of Crete are comparable to onshore stations. Final earthquake locations were computed by running VELEST in 'single event mode'.

An attempt to solve for independent S-velocity models was done using v_p-models with an rms misfit not larger than 0.13 s and a constant v_p/v_s ratio of 1.78 for starting v_s-models. Because the 10 best v_p-models show very similar velocities in the depth range between 15 and 35 km (Fig. 5a) we chose all models with an rms misfit $\leq 0.13\,s$, i.e. the best 52 models, to better sample the velocity space. Results from this inversion attempt show that in the best constrained depth range between 15 and 35 km the v_p/v_s ratio is almost constant around 1.78-1.80 (Fig. 5c). Towards shallower depths high v_p/v_s ratios with values above 2 and sometimes as high as 3.5 may indicate the presence of the slow, possibly water saturated, sediments in the south. For depths compatible with the African mantle lithosphere rather low v_p/v_s ratios of less than 1.7 are found. However, the results from the v_s-model inversion are not very well constrained and thus are not considered in the further discussion.

3.3 Probabilistic Event Localization

In order to investigate the influence of the slab and the thick sedimentary cover in the southern part of the network on the seismicity distribution, a simple 3-D velocity model based on a priori velocity information from refraction seismic studies (Bohnhoff et al., 2001; Brönner, 2003) as well as seismological receiver function and surface wave dispersion studies (Endrun et al., 2004) was generated. The velocity model, which consists of cubic cells with side lengths of 1 km, has a dimension of 360 x 275 x 91 kilometres in longitude, latitude and depth, respectively and starts

one kilometre above sea-level to contain all recording stations within its dimensions. Islands are modelled as blocks being superimposed on a background velocity model. The horizontal curvature of the subduction zone is neglected in this simple approach. This velocity model (Fig. 6) also includes the effect of the thick sedimentary cover in the south by incorporating low P-velocities and large v_p/v_s ratios indicated by the above discussed inversion approach and a gently dipping African slab. This model was used in conjunction with the probabilistic NonLinLoc earthquake localization program (Lomax, 2000), using the Oct-tree search mode, to solve for earthquake hypocentres. This procedure starts with a global sampling of the search space using a coarse grid and than finds the maximum likelihood hypocentre by mapping the probability density function of the earthquake location by an increasingly finer sampling of the search space. This approach samples a wider range of the solution space than the gradient methods and allows an estimation of the location uncertainties. Station corrections for this model were calculated as the mean travel time residual at the respective station and then applied in the final event localization run.

The area in which seismicity can be located with this scheme is truncated by the edges of the velocity model which are found roughly at 33.25 and 35.68°N and 23.25 and 27.2°E. These borders are not exactly parallel to meridians because a rectangular grid with constant grid spacing is transferred to geographical coordinates. Earthquakes outside these boundaries are projected onto the edges of the velocity model with large rms values.

Finally, the probabilistic NonLinLoc routine was initialized with the minimum 1-D velocity model and corresponding station corrections and the Oct-tree search algorithm was used to calculate event hypocentres. A mapview of the resulting event distribution for this localization approach can be found in Fig. 7.

3.4 Model Performances and Localization Uncertainties

The general microseismicity distribution remains the same for all four localization approaches (Figs. 10,11). This indicates the stability of the localization results and that the general event distribution is not very sensitive with respect to the choice of different, reasonable velocity models and the localization approach. The influence of the slab on the seismicity distribution is small which can be expected because hardly

any intermediate depth activity is observed and most of the seismicity is found either within the crust or at the plate contact and is thus not very sensitive to the geometry of the subducting African lithosphere. This can be seen when comparing the results for the 3-D velocity model (Fig. 11c) with the minimum 1-D velocity model (Fig. 11d) for the area north of the Pliny trench. Locations in this area are very similar for the 1-D and 3-D case.

Towards the south, however, the influence of the low velocities and the high v_p/v_s ratios of the sedimentary layers incorporated in the 3-D velocity model are clearly evident by the much shallower depths of the hypocentres in the 3-D case (Figs. 10c,11c) when compared with the minimum 1-D solution (Figs. 10d,10d). This tendency towards shallower depths is also evident when comparing the minimum 1-D locations with station corrections with the initial event locations (e.g. Figs. 11a,b). Also, the large positive station residuals calculated in the inversion for stations in the south (Fig. 5d) hint at low velocities in that area and thus possibly shallower hypocentral depths. A thick sedimentary cover of up to 10 km, which was found in refraction seismic studies of this region (Bohnhoff, 2001; Brönner, 2003), may be responsible for the locally reduced data quality due to scattering and subsequent lower SNR due to damping. The velocity model resulting from the VELEST inversion is generally slower than the initial model derived from the onshore network by Meier et al. (2004a) (Fig. 4) as expected from the fact that the lower velocities in the upper layers in the southern offshore region must somehow be incorporated in an average 1-D velocity model.

Although the general event distribution is the same for all localization approaches quantifiable differences between them do exist. As expected, the minimum 1-D velocity model with corresponding station corrections in conjunction with a gradient method for event localization performs significantly better than the starting velocity model using the same localization method (Fig. 8a,b). The computed average rms misfit for the 435 events used in the inversion is 0.26 s when using the minimum 1-D velocity model, a v_p/v_s ratio of 1.78 and corresponding station corrections. This is a significant improvement compared with the average misfit of 0.35 s obtained with the initial velocity model. Trying to solve for independent S-velocity models does not significantly improve this misfit. Due to the fact that a rather complicated model with sharp changes in the v_p/v_s ratio is needed to obtain a similar misfit, 0.24 s compared to the 0.26 s for a constant v_p/v_s ratio, this velocity model with independent S-velocities is rejected.

Despite the incorporation of low velocities and large v_p/v_s ratios in the southern area the 3-D velocity model does not perform better than the minimum 1-D velocity model with corresponding station corrections when applying a probabilistic localization scheme to both velocity models, although there are several events with very small rms values for the 3-D model. This might be due to the fact that the 3-D velocity model is too simple for the complicated geometry in this curved subduction zone with its local structural heterogeneities. Furthermore, the strong lateral velocity changes make the localization procedure more sensitive to small changes in hypocentral parameters. This effect can be seen in the larger scatter of the hypocentres when compared to the minimum 1-D solution (Figs. 11c,d). Furthermore, the maximum axis of the error ellipsoid tends to be larger than in the 1-D case (Figs. 8c,d).

Event locations obtained with the minimum 1-D velocity model and a probabilistic approach also show a smaller scatter in the hypocentre distribution (Fig. 11d) than those obtained by a gradient method (Fig. 11b). We performed a synthetic test to quantify this visual observation. Synthetic traveltimes were calculated for an event roughly at the centre of the offshore network for 11 stations of the amphibian network surrounding this hypocentre. These synthetic travel times were perturbed with random noise. The added travel-time error was normally distributed with a standard deviation of 0.3 s for the P-wave travel time and 0.6 s for the S-wave travel time. Then the event was located using these perturbed travel times. This procedure was done 200 times for the linear gradient approach as well as for the probabilistic approach. While both localization schemes show comparable performances with respect to the horizontal directions the probabilistic approach is able to better constrain the depth of the event. Fig. 9 shows the result of the test with respect to the recovered depth. The probabilistic approach (Fig. 9b) exhibits a standard deviation of 1.25 km for the 200 location runs compared to the 1.53 km obtained for the gradient method (Fig. 9a) and avoids termination in local minima. This contrasts with the result for the gradient method which exhibits a pronounced local maximum at a velocity step at about 34 km depth. Locations obtained by applying a probabilistic event localization scheme with the minimum 1-D velocity model and corresponding station corrections seem to be on average better constrained than those obtained by the other approaches. Thus, the following discussion of the microseismicity distribution is based on the results from the minimum 1-D model with corresponding station corrections used in the probabilistic localization scheme.

Location accuracy for well resolved events recorded by the network is of the order of less than 5 km for horizontal directions and approximately worse by a factor of two in vertical direction. An idea of the expected error ellipsoids of events recorded by the network can be gained from Fig. 12. In this figure a subset of the final earthquake catalogue is plotted with error ellipsoids obtained by mapping the probability density function for the minimum 1-D model in probabilistic earthquake localization mode. The chosen subset is from a single deployment phase which guarantees that the station configuration does not change. A time period exhibiting activity throughout the whole study region was chosen. Obviously, the vertical error is considerably larger than the horizontal one for less well constrained events and those at the edges or outside the amphibian network. A general increase of the error ellipsoid is observed for events locating towards the southern and eastern edges of the amphibian network. The larger error ellipsoids observed for events locating in these areas might be explained by a worse fit of the velocity model to the true situation and a less dense station coverage. In addition, the data quality of the southern stations is not as good as that of the northern ones making proper phase identification and picking more difficult. The horizontal location accuracy however remains high for events in the region of the Pliny trench as indicated by well constrained events in that region allowing a clear localization of the seismogenic zones while it is getting increasingly worse towards the south in the region of the Strabo trench (Fig. 12).

4 Discussion

The microseismic activity in the forearc of the HSZ south of central and eastern Crete occurring between July 2003 and June 2004 was studied by means of an amphibian network covering the entire transtensional on- and offshore graben system in that area. In the following the most reliable hypocentre locations obtained with the probabilistic event localization and using the minimum 1-D velocity model with corresponding station corrections are used to interpret the microsmicity distribution.

4.1 Microseismicity offshore of Crete

Prominent crustal microseismic activity within the Aegean plate in the area of the Ptolemy trench was observed throughout the whole observation period (Fig. 14a). This activity close to the southern coast of Crete was also identified in earlier microseismicity studies of the region (Delibasis et al., 1999; Meier et al., 2004b; Becker et al., 2006) using land-based seismic networks. Combining our findings with the ISC catalogue (Engdahl et al., 1998) which also lists seismic events with intermediate magnitudes in that area we conclude that the Ptolemy structure constitutes a continuously seismically active feature in the Aegean crust. This intra-crustal activity extends from near surface depths down to the presumed plate interface at approximately 40 km depth and was traced by this study in west-east direction from offshore Messara in the west (Fig. 10) up to the eastern shoreline of Crete and possibly even further east towards the island of Karpathos (Fig. 7). In a study emphasizing basin-scale structural relations ten Veen and Kleinspehn (2003) suggest an active transtensional regime on- and offshore central and eastern Crete resulting in forearc slivers separated from the Cretan block due to internal deformation of the Aegean crust in that area. They arrive at this conclusion by analyzing motions on 070° sinistral faults in the Messara region. The development of these slivers is explained by the blocking of the further outward expansion of the Aegean plate boundary in western Crete due to the incipient collision with Africa and the simultaneous expansion of the Aegean crust by the stretching of the Cretan-Rhodes forearc in the east caused by the still active slab rollback in that area. Although findings of this study have been questioned (Ring and Brachert, 2003) seismic studies show similar wedge-shaped sedimentary basins in the vicinity of the Ptolemy and Pliny trench (Bohnhoff et al., 2001) suggesting a similar origin of the two structures. Fault plane solutions (Fig. 1) and analysis of GPS measurements (Kahle et al., 2000) indicate sinistral motions in the area of the Pliny and Strabo trenches. The presence of microearthquake clusters found in earlier studies (Becker et al., 2006) suggests that the Ptolemy trench represents a zone of crustal weakness allowing the ascent of fluids from the plate contact.

Towards the south between the Ptolemy and the Pliny trenches we observe a sharp drop of crustal seismicity within the overriding Aegean plate and seismicity is nearly exclusively found at the presumed plate interface (Figs. 10,11). The absence of intra-plate microseismic activity between the Ptolemy and Pliny trenches is in

contrast to the rather strong microseismic activity observed further south between the Pliny and Strabo trenches. This absence of microseismic activity might indicate that no or only very little internal deformation is occurring at this part of the upper plate. Therefore, the microseismicity distribution found in this study suggests that the Ptolemy and Pliny trenches are the borders of a forearc sliver separated from the rest of the Aegean forearc. This observation is supported by the interpretations of ten Veen and Kleinspehn (2003). Whether the Strabo trench towards the south has a similar character as the Pliny trench can not be finally resolved due to inferior location precision in this region. The microseismicity located at crustal depth between the Pliny and Strabo trench (Fig. 7) which agrees with event locations of intermediate magnitude seismicity of the ISC catalogue (Fig. 2), however, indicates that the region between the Pliny and Strabo trenches shows strong internal deformation and can not be interpreted as a further forearc sliver. These observations are in agreement with the results of swath bathymetry and seismic reflection profiles (Huguen et al., 2001) which observed faulted, locally uplifted basement blocks south of the Pliny trench. According to Huguen et al. (2001) this southernmost domain of the Cretan continental margin is disconnected from its northern part by the Pliny trench. Microseismic activity in this region is comparable to that observed in the north at the Ptolemy trench when taking into account the higher completeness magnitude of the southern region (Fig. 14b) of about $M_L = 2.5$ when compared to the value of 1.5 in the area of the Ptolemy trench and the high a- and b-values observed at the Pliny and Strabo trenches (Figs. 14c,d). These high b-values serve as a further indicator that this area is broken into several smaller sub-blocks accommodating the deformation in this part of the forearc. A- and b-values calculated in this study account for changes in the completeness magnitude (M_c) by determining a separate M_c for each studied grid point. However, due to the lower event density in the south the resolution of the a- and b-value maps decreases in this region because a larger area has to be sampled to obtain enough events for a reliable determination of the a- and b-values. Furthermore, the values obtained only cover a time interval of slightly more than 10 months and present a snapshot in time which might be influenced by cluster activity in one part or exceptionally large events in other regions. Nevertheless, the a- and b-value results presented in this study are in agreement with other observations and thus seem to support the presented conclusions. The strong microseismic activity indicating the seismogenic part of the plate contact between the African and Aegean plates, which has its southern termination below the

Strabo trench, extends northwards up to the southern coast of Crete over a width of about 100 km (Fig. 15). The northern part of the interplate seismicity was also observed by earlier land-based temporary networks (Delibasis et al., 1999; Meier et al., 2004a) while these studies were not able to detect its southern termination due to the lack of offshore stations. This interplate seismicity is rather evenly distributed and no locked zones indicating possible areas of stress accumulation were detected. The only marked deviation from this event distribution is a cluster of events in the region of the western termination of the Pliny trench around 34.4°N/25°E (Figs. 7,10d). This region of elevated microseismic activity is also found in the instrumental ISC catalogue (Fig. 2) and can be recognized in the bathymetry as a pronounced depression (Fig. 1). Striking is also the absence of microseismic and intermediate magnitude activity towards the west of this cluster (Figs. 2, 7). This behaviour might be explained by a retreat of the forearc sliver bounded by the Ptolemy and Pliny trenches in north-eastward direction caused by the same mechanism of stretching of the Cretan-Rhodes forearc in south-eastward direction and blocking of a further expansion to the west due to incipient collision with Africa as discussed above. If this assumption is correct, the observed seismic activity would delineate the south-western termination of this forearc sliver. Gravity surveys in the region of the forearc find a low corresponding to the seismically quiet region towards the west of the cluster activity. This negative anomaly is interpreted as an effect of deep reaching sediments (Casten & Snopek, 2006) supporting the assumption that the retreat of the forearc sliver created a void which was subsequently filled with sediments but still shows an expression in the bathymetry.

B-values calculated in this study for regions dominated by interplate seismicity tend to be lower than those observed for areas dominated by the intra-crustal seismicity of the trenches (Fig. 14c) with higher values in the area of the Pliny and Strabo trenches than for the Ptolemy trench. This observation is in agreement with an earlier study that found cluster activity in the Ptolemy trench which was linked to fluid activity (Becker et al., 2006) suggesting that similar fluid related activity is also present in the area of the Pliny and Strabo trenches. Furthermore, higher b-values generally correlate with regions where large events are absent (Wyss, 2001). This might also explain the absence of historic seismicity with large magnitudes in the area of the Pliny and Strabo trenches which exhibit considerable current intermediate magnitude seismicity (Figs. 1 , 2). Possibly, this region is accommodating the relative

plate motions by numerous small and intermediate rather than few large magnitude events. An alternative explanation might be that no extended continuous fault surfaces exist. An indication for this hypotheses can be found in the already mentioned swath mapping and reflection seismic data of the region (Huguen et al., 2001) which identify separate, sometimes uplifted basement blocks. In contrast, the Ptolemy trench with its smaller b-values already showed its potential to generate large magnitude events (Fig. 1). Another explanation might be that the historic catalogue is biased, containing preferentially events close to the inhabited island of Crete. This, however, fails to explain the difference in the b-values observed in the study.
The accretionary complex to the south of the Strabo trench is practically devoid of any microseismic activity. Also, the presumed plate contact between the African and the Aegean plates south of the Strabo trench exhibits aseismic behaviour.

4.2 Microseismicity beneath Crete

Crustal seismicity below the island of Crete is less pronounced than to the south of the island. One of the seismically most prominent areas is the Messara graben, which is a roughly east-west striking half-graben structure at the south coast of Crete north of station APEZ (Figs. 2,13). There, fault scarps cutting Quaternary deposits were observed (Monaco and Tortorici, 2004) and seismicity with magnitudes of up to M_w6.0 is reported (Papazachos et al., 2000). From the inset of Fig. 13 which depicts the activity in this region at high spatial resolution indications for a southward dipping structure coalescing with the seismicity of the Ptolemy trench at a depth of 20 km can be found. Below this depth the now merged activity can be traced down to the presumed depth of the plate contact at 40 km. The observed microseismicity distribution might indicate a connection between the Ptolemy trench and a southward dipping structure outcropping in the Messara basin. North of this structure sporadic microseismicity is observed down to depths of 40 km. This contrasts with observations further east along the Ptolemy trench (Fig. 11) were microseismic activity north of the Ptolemy trench is restricted to the upper 20 km of the continental crust. Microseismic activity observed in the Ierapetra graben onshore Crete (Fig. 13), a north-north-east south-south-west trending structure, is confined to the upper 20 km of the crust (Fig. 11d) and does not reach down to depths of the lower continental crust. Also, a roughly north-south

trending structure adjacent to the south-east coast of Crete with hypocentral depths between 10 and 30 km was active during the observation period (Fig. 13). Active quaternary normal faults known from geologic and sea-beam observations (Angelier et al., 1982; Armijo et al., 1992) are reported for these areas as well. The activation of these N-S to NNE-SSW trending normal faults is in agreement with the current stress field in eastern Crete (Bohnhoff et al., 2005) and consistent with fault-plane solutions indicating E-W extension in the region east of Crete (Fig. 1). Generally, the region east of the Ierapetra graben exhibits stronger seismic activity than the region to the west. However, there are two spots of significant earthquake clustering to the west of the Ierapetra graben in the vicinity of the permanent broad-band station at Kristallenia (labeled KRIS in Fig. 2) and further north at the coast. These locations exhibit cluster-like activity with magnitudes up to $M_L = 3.5$ (Fig. 7).
The termination of the interplate seismicity coincides with the southern shore of Crete and indicates that the plate contact south of Crete is seismically coupled whereas it is decoupled below and north of Crete. As a consequence, Crete is located above the updip limit of the decoupled plate interface and thus the uplift of Crete (e.g. Meulenkamp et al., 1994) hints at return flow above the slab in the region of the decoupled interface (Fig. 15). Furthermore, seismicity within the Aegean lithosphere below Crete is low at depths below about 20 km (Figs. 11d, 15) pointing to rather ductile deformation of the overriding plate in contrast to brittle behaviour at shallower depths. These observations are in good agreement with numerical modellings of rheological properties of the plate contact in the forearc (e.g. Gerya et al. 2002; Gerya and Stöckhert, 2006). These modellings predict (1) rapid return flow of metamorphic rocks, including hydrated mantle material, along the hanging wall of the subducted slab that spread out beneath the forearc and (2) ductile behaviour of the plate contact and deeper parts of the overriding plate in the region of the forearc high.

4.3 Intermediate depth seismicity

Only little intermediate depth seismic activity within the subducting African lithosphere was observed during the study period. Events located directly north of the Pliny trench below the oceanic crust are not very well constrained (Fig. 15). Thus, we can not finally resolve whether this activity might be linked to the slab bending

expected in this region.
The deepest events reaching more than 100 km were located north-east of Crete. They are most likely associated with the Benioff zone, i.e. the subducting slab. Activity in the slab below the island of Crete was also very sparse with only a few events located in the depth range between 40 and 80 km. Interestingly, intermediate depth seismicity originating in the subducting African slab further to the north with depths exceeding 100 km exhibits high data quality at OBS stations close to Crete (Fig. 3b) suggesting that the subducting slab acts as a waveguide as suggested by earlier studies on the attenuation of seismic signals and the distribution of macroseismic intensities in the region (Papazachos and Comninakis, 1971). These intermediate depth events might be linked to processes within the slab like bending, dehydration and phase changes.

5 Conclusions

We present results from an amphibian passive seismic field campaign in the area of SE Crete and adjacent offshore region. OBS stations close to the south coast of Crete exhibit high data quality comparable to adjacent land stations while stations further to the south show low SNRs with emergent onsets and very long signal coda. This behaviour is presumably caused by the thick water-filled sedimentary cover in this region.
The general microseismicity distribution is not very sensitive to reasonable changes in the velocity model or different localization techniques. Achieved location accuracy is of the order of 5 km horizontally and slightly worse than that in vertical direction for well constrained events. The most reliable event locations were obtained by performing a probabilistic event localization using a 1-D velocity model and corresponding station corrections obtained by simultaneous inversion.
Strong crustal microseismic activity is observed along the entire length of the Ptolemy trench and further south in the region between the Pliny and Strabo trenches while the crustal region in between is almost devoid of microseismic activity. We suggest that this region constitutes a forearc sliver which moves as a rigid block accommodating relative motions along the transtensional structures of the Ptolemy and Pliny trenches. The seismogenic part of the plate contact has a width of approximately 100 km from

the region of the Strabo trench in the south to roughly the south coast of Crete in the north while the plate contact below Crete and south of the Strabo trench exhibits aseismic behaviour and thus seems to be seismically decoupled. Microseismic activity at the plate contact is rather evenly distributed and no indications for locked zones and corresponding stress accumulations were observed during the observation period. Seismic activity below Crete is mainly confined to the upper 20 km indicating a ductile behaviour of the lower crust. In the region of the Messara half-graben onshore central Crete a southward dipping seismogenic structure is identified which coalesces with the seismicity of the Ptolemy trench at a depth of 20 km. The general behaviour of a ductile lower crust as well as the location of the downdip limit of the seismogenic zone of the plate contact below the south coast of Crete are in agreement with the idea of a return flow of metamorphic material. This material is supposed to flow along the hanging wall of the subducted slab spreading out beneath the forearc and contributing to the rapid uplift of Crete.

Acknowledgements

We thank A. Pino and an anonymous reviewer for their thoughtful comments and their constructive criticism that were very helpful in improving the manuscript. GEOPRO GmbH, Hamburg, conducted the deployment and recovery of the OBS stations. We thank M. Rische, B. Klotz and L. Kühne for their invaluable help during the field operation of the short period network. N. Economou and A. Vafidis of the University of Chania, Crete, provided support for the installation, maintenance and demobilization of the short period network.

Waveform data from the permanent broad-band stations were provided by the GeoForschungsZentrum Potsdam through the GEOFON project. The National Observatory of Athens (NOA) provided waveforms from broad-band stations installed in the vicinity of Crete. Fault plane solutions were provided by the Harvard CMT project (http://www.globalcmt.org) and obtained from the web page of the project on 26 Feb 2009. The VELEST source code was provided by E. Kissling. The code for the probabilistic earthquake location software (NLLoc) was made available by A. Lomax. Magnitude completeness and b-value maps were prepared using the zmap software which was written and provided by M. Wyss, S. Wiemer and R. Zuniga. Figs. 1 and 6 were prepared using GMT software. We greatly acknowledge the free availability of all

these software packages. The work was supported by the German Research Foundation (DFG) within the collaborative research center 526 "Rheology of the Earth: From the Upper Crust to the Subduction Zone".

References

J. Angelier, N. Lyberis, X. LePichon, E. Barrier, and P. Huchon. The tectonic development of the Hellenic arc and the sea of Crete. *Tectonophysics*, 86:159–196, 1982.

R.H. Armijo, H. Lyon-Caen, and D. Papanastassiou. East-west extension and Holocene normal-fault scarps in the Hellenic arc. *Geology*, 20:491–494, 1992.

D. Becker. Mikroseismizität und Deformation der Kruste Ostkretas. 2000. Diploma Thesis, in German.

D. Becker, T. Meier, M. Rische, M. Bohnhoff, and H.-P. Harjes. Spatio-temporal microseismicity clustering in the Cretan region. *Tectonophysics*, 423:3–16, 2006.

M. Bohnhoff, J. Makris, G. Stavrakakis, and D. Papanikolaou. Crustal investigation of the Hellenic subduction zone using wide aperture seismic data. *Tectonophysics*, 343: 239–262, 2001.

M. Bohnhoff, T. Meier, and H.P. Harjes. Stress regime at the Hellenic Arc from focal mechanisms. *J. Seismology*, 9:341–366, 2005.

M. Brönner. *Untersuchung des Krustenaufbaus entlang des Mediterranen Rückens abgeleitet aus geophysikalischen Messungen*. PhD thesis, Universität Hamburg, 2003. In German.

U. Casten and K. Snopek. Gravity modelling of the Hellenic subduction zone - a regional study. *Tectonophysics*, 417:183–200, 2006.

G. Cifci, A. Limonov, L. Dimitrov, and V. Gaianov. Mud Volcanoes and Dome-Like Structures at the Eastern Mediterranean Ridge. *Mar. Geophys. Res.*, 19:421–438, 1997.

J.B. de Chabalier, H. Lyon-Caen, A. Zollo, A. Deschamps, P. Bernard, and D. Hatzfeld. A detailed analysis of microearthquakes in western Crete from digital three-component seismograms. *Geophys. J. Int.*, 110:347–360, 1992.

N. Delibasis, M. Ziazias, N. Voulgaris, T. Papadopoulos, G. Stavrakakis, D. Papanastassiou, and G. Drakatos. Microseismic activity and seismotectonics of the Heraklion area (central Crete Island, Greece). *Tectonophysics*, 308:237–248, 1999.

J. Dercourt, L.P. Zonenshain, L.-E. Ricou, V.G. Kazmin, X. LePichon, A.L. Knipper, C. Grandjacquet, I.M. Sbortshikov, J. Geyssant, C. Lepvrier, D.H. Pechersky, J. Boulin, J.-C. Sibuet, L.A. Savostin, O. Sorokhtin, M. Westphal, M.L. Bazhenov, J.P. Lauer, and B. Biju-Duval. Geological evolution of the Tethys belt from the Atlantic to the Pamirs since Lias. *Tectonophysics*, 123:241–315, 1986.

B. Endrun, T. Meier, M. Bischoff, and H.-P. Harjes. Lithospheric structure in the area of Crete constrained by receiver functions and dispersion analysis of Rayleigh phase velocities. *Geophys. J. Int.*, 158:592–608, 2004.

E.R. Engdahl, R. van der Hilst, and R. Buland. Global teleseismic earthquake relocation with improved travel times and procedures for depth determination. *Bull. Seismol. Soc. Am.*, 88:722–743, 1998.

C. Facenna, L. Jolivet, C. Piromallo, and A. Morelli. Subduction and the depth of convection in the Mediterranean mantle. *J. Geophys. Res.*, 108, 2003. doi:10.1029/2001JB0011690.

J. Galindo-Zaldivar, L. Nieto, and J. Woodside. Structural features of mud volcanoes and the fold system of the mediterranean ridge, south of crete. *Mar. Geol.*, 132: 95–112, 1996.

W.K. Gealey. Plate tectonic evolution of the Mediterranean - Middle East region. *Tectonophysics*, 155:285–306, 1988.

T.V. Gerya and B. Stöckhert. 2-D numerical modeling of tectonic and metamorphic histories at active continental margins. *Int. J. Earth Sciences*, 2006. in press.

T.V. Gerya, B. Stöckhert, and A.L. Perchuk. Exhumation of high-pressure metamorphic rocks in a subduction channel - a numerical simulation. *Tectonics*, 21:6–1 – 6–19, 2002.

W. Hanka and R. Kind. The GEOFON Program. *Annali di Geofisica*, 33:1060–1065, 1994.

D. Hatzfeld, M. Besnard, K. Makropoulos, and P. Hatzdimitriou. Microearthquake seismicity and fault-plane solutions in the southern Aegean and its geodynamic implications. *Geophys. J. Int.*, pages 799–818, 1993.

P. Huchon, N. Lyberis, J. Angelier, X. LePichon, and V. Renard. Tectonics of the Hellenic Trench: A Synthesis of Sea-Beam and Submersible Observations. *Tectonophysics*, 86:69–112, 1982.

C. Huguen, J. Mascle, E. Chaumillon, J.M. Woodside, J. Benkhelil, A. Kopf, and A. Volksonkaia. Deformation styles of the eastern Mediterranean Ridge and surroundings from combined swath mapping and seismic reflection profiling. *Tectonophysics*, 343:21–47, 2001.

H.-G. Kahle, M. Cochard, Y. Peter, A. Geiger, R. Reilinger, A. Barka, and G. Veis. GPS-derived strain rate field within the boundary zones of the Eurasian, African and Arabian Plates. *J. Geophys. Res.*, 105:23353–23370, 2000.

A. A. Kiratzi and B. C. Papazachos. Magnitude scales for earthquakes in Greece. *Bull. Seism. Soc. Am.*, 74:969–985, 1984.

E. Kissling, W. Ellsworth, D. Eberhart-Phillips, and U. Kradolfer. Initial reference models in local earthquake tomography. *J. Geophys. Res.*, 99:19635–19646, 1994.

F. W. Klein. User's Guide to HYPOINVERSE-2000, a Fortran Program to Solve for Earthquake Locations and Magnitudes. Technical Report 02-171, U.S. Dep. Int., Geological Survey, 2002.

A.J. Kopf. Significance of mud volcanism. *Rev. Geophys.*, 40, 2002. doi:10.1029/2000RG000093.

S.A. Kovachev, I.P. Kuzin, and S.L. Soloviev. Spatial Distribution of Microearthquakes in the Frontal Part of the Hellenic Arc according to Observations of Bottom Seismographs. *Geotektonika*, 25:155–160, 1991.

S.A. Kovachev, I.P. Kuzin, and S.L. Soloviev. Microseismicity of the frontal Hellenic arc according to OBS observations. *Tectonophysics*, 201:317–327, 1992.

M. Laigle, M. Sachpazi, and A. Hirn. Variation of seismic coupling with slab detachment and upper plate structure along the western Hellenic subduction zone. *Tectonophysics*, 391:85–95, 2004.

S. Lallemant, C. Truffert, L. Jolivet, P. Henry, N. Chamot-Rooke, and B. de Voogd. Spatial transition from compression to extension in the Western Mediterranean Ridge accrettionary complex. *Tectonophysics*, 234:33–52, 1994.

A. Lomax, J. Virieux, P. Volant, and C. Berge-Thierry. Probabilistic earthquake location in 3D and layered models. In C.H. Thurber and N. Rabinowitz, editors, *Advances in seismic event location*, Dordrecht, Netherlands, 2000. Kluwer Academic Publishers.

K.C. Makropoulos and P.W. Burton. Greek tectonics and seismicity. *Tectonophysics*, 106:275–304, 1984.

J. Mascle, C. Huguen, J. Benkhelil, N. Chamot-Rooke, E. Chaumillon, J.P. Foucher, R. Griboulard, A. Kopf, G. Lamarche, A. Volkonskaia, J. Woodside, and T. Zitter. Images may show start of European-African plate collision. *EOS*, 80 (37):421,425,428, 1999.

S. McClusky, S. Ballassanian, A. Barka, C. Demir, S. Ergintav, I. Georgiev, O. Gurkan, M. Hamburger, K. Hurst, H. Kahle, K. Kastens, G. Kekelidze, R. King, V. Kotzev, O. Lenk, S. Mahmoud, A. Mishin, M. Nadariya, A. Ouzounis, D. Paradissis, Y. Peter, M. Prilepin, R. Reilinger, I. Sanli, H. Seeger, A. Tealeb, M.N. Toksöz, and G. Veis. Global Positionng System constraints on plate kinematics and dynamics in the eastern Mediterranean and Caucasus. *J. Geophys. Res.*, 105:5695–5719, 2000.

T. Meier, M. Rische, B. Endrun, A. Vafidis, and H.-P. Harjes. Seismicity of the Hellenic subduction zone in the area of western and central Crete observed by temporary local seismic networks. *Tectonophysics*, 383:149–169, 2004a.

T. Meier, K. Dietrich, B. Stöckhert, and H.-P. Harjes. One dimensional models for shear wave velocity for the Eastern Mediterranean obtained from the inversion of Reighley wave phase velocities and tectonic implications. *Geophys. J. Int.*, 156:45–58, 2004b. doi:10.1111/j.1365-246X.2004.92121.x.

T. Meier, D. Becker, B. Endrun, M. Rische, M. Bohnhoff, B. St öckhert, and H.-P. Harjes. A model for the Hellenic subduction zone in the area of Crete based on seosmological investigations. In T. Taymaz, Y. Yilmaz, and Y. Dilek, editors, *The Geodynamics of the Aegean and Anatalia*, pages 183–199, Geological Society, London, Special Publications, 291, 2007.

J.E. Meulenkamp, G.J. van der Zwaan, and W.A. van Wamel. On Late Miocene to recent vertical motions in the Cretan segment of the Hellenic arc. *Tectonophysics*, 234:53–72, 1994.

C. Monaco and L. Tortorici. Faulting and effects of earthquakes on Minoan archological sites in Crete (Greece). *Tectonophysics*, 382:103–116, 2004.

B.C. Papazachos. Large Seismic Faults in the Hellenic Arc. *Annal. di Geophys. XXXIX*, 5:891–903, 1996.

B.C. Papazachos and P.E. Comninakis. Geophysical and tectonic features of the Aegean arc. *J. Geophys. Res.*, 76:8517–853, 1971.

B.C. Papazachos and C. Papazachou. *The earthquakes of Greece*. Ziti Publ., 1997.

B.C. Papazachos, C.A. Papaioannou, C.B. Papazachos, and A.S. Savvaidis. Rupture zones in the Aegean region. *Tectonophysics*, 308:205–221, 1999.

B.C. Papazachos, P.E. Comninakis, B.G. Karakaisis, B.G. Karakostas, C.A. Papaioannou, C.B. Papazachos, and E.M. Scordilis. *A catalog of earthquakes in Greece and Surrounding Area for the Period 550BC-1999*. Geophysics Laboratory, 2000a. University of Thessaloniki.

B.C. Papazachos, V.G. Karakostas, C.B. Papazachos, and E.M. Scordilis. The geometry of the Wadati-Benioff zone and the lithospheric kinematics in the Hellenic arc. *Tectonophysics*, 319:275–300, 2000b.

C.B. Papazachos and G. Nolet. P and S deep velocity structure of the Hellenic area obtained by robust nonlinear inversion of travel times. *J. Geophys. Res.*, 102:8349–8367, 1997.

X. Le Pichon, N. Lyberis, J. Angelier, and V. Renard. Strain distribution over the east Mediterranean Ridge: A synthesis incorporating new sea-beam data. *Tectonophysics*, 86:243–274, 1982.

X. Le Pichon, N. Chamot-Rooke, S. Lallement, R. Noomen, and G. Veis. Geodetic determination of the kinematics of central Greece with respect to Europe: Implications for the eastern Mediterranean tectonics. *J. Geophys. Res.*, 100:12675 –12690, 1995.

P. A. Pirazzoli. Uplift of Ancient Greek Coastal Sites: Study Methods and Results. In S. Stiros and R. E. Jones, editors, *Archaeoseismology*, pages 237–244, Athens, Greece, 1996.

U. Ring and T. C. Borchert. Discussion on incipient continental collision and plate-boundary curvature: Late Pliocene-Holocene transtensional Hellenic forearc, Crete, Greece. *J. Geol. Sci.*, 160:819–824, 2003.

E.A. Robinson. *Statistical communication and detection with special reference to digital data processing of radar and seismic signals.* Charles Griffin and Company, Ltd., 1967. London.

B. Shaw, N.N. Ambraseys, P.C. England, M.A. Floyd, G.J. Gorman, T.F.G. Highman, J.A. Jackson, J.-M. Nocquet, C.C. Pain, and M.D. Piggott. Eastern Mediterranean tectonics and tsunami hazard inferred from the AD 365 earthquake. *Nature Geoscience*, 1:268–276, 2008.

W. Spakman, S. van der Lee, and R. van der Hilst. Travel-time tomography of the European-Mediterranean mantle down to 1400 km. *Phys. Earth Planet. Int.*, 79: 3–74, 1993.

S.C. Stiros. The AD 365 Crete earthquake and possible seismic clustering during the fourth to sixth centuries AD in the Eastern Mediterranean: a review of historical and archaeological data. *J. Struct. Geol.*, 23:545–562, 2001.

J.H. ten Veen and K.L. Kleinspehn. Incipient continental collision and plate-boundary curvature: Late Pliocene-Holocene transtensional Hellenic forearc. *J. Geol. Soc.*, 160: 161–181, 2003.

J.H. ten Veen and P.T. Meijer. Late Miocene to recent tectonic evolution of Crete (Greece): geological observations and model analysis. *Tectonophysics*, 298:191–208, 1998.

S.N. Thomson, B. Stöckhert, and M.R. Brix. Thermochronology of the high-pressure metamorphic rocks of Crete, Greece: Implications for the speed of tectonic processes. *Geology*, 26:259–262, 1998.

M. Wyss. Locked and creeping patches of the Hayward fault, California. *Geophys. Res. Lett.*, 28:3537–3540, 2001.

6 Captions

Fig. 1: Historic seismicity and Harvard CMT solutions calculated for the convergent plate boundary of the Hellenic Subduction Zone. Major seismicity (black and white triangles) with magnitudes $M_w \geq 6.0$ spans the time period 550 BC - 1999 AD (Papazachos et al., 2000) while beach balls represent fault plane solutions for events between 1977 and 2008 (www.globalcmt.org). Solid black lines indicate the locations of the Ionian, Ptolemy, Pliny and Strabo trenches as seen in the bathymetry and arrows indicate sense of displacement of the transtensional structures (e.g. Kahle et al., 2000; tenVeen and Kleinspehn, 2003). Broken black line indicates the presumed crustal ocean- continent transition. Mud volcano fields in the accretionary prism south of the Pliny and Strabo trenches are indicated by broken magenta lines (Galindo-Zaldivar et al., 1996; Cifci et al., 1997). Plate velocities and directions of movement of the African and Aegean plate are indicated by arrows. Velocities are relative to a stable Eurasian reference frame. See McClusky et al. (2000) for details.

Fig. 2: Relocated seismicity according to the ISC catalogue during the time period 1963-1999 (Engdahl et al., 1998) for the region around Crete (circles) and microseismicity located by temporary onshore networks (Meier et al., 2004a; Becker, 2000; blue dots). The configuration of the amphibian seismic network evaluated in this study is superimposed. Triangles mark the OBS locations of LIBNET, diamonds mark temporary short period onshore stations and inverted triangles mark permanent broad-band stations from the GEOFON-, NOA- and MEDNET-networks. Colour-coding of the symbol outline indicates begin of recording while the colour in the symbols interior indicates the end of recording for the respective station. Corresponding colour-scale is given in the lower part of the Figure. Inset: Hypocentres of ISC catalogue events (dark gray dots; Engdahl et al., 1998) and microseismicity recorded with a network on eastern Crete (light gray dots; Becker, 2000) projected on a plane along profile AA'. Events with a distance of up to 20 km from the profile are used for the projection.

Fig. 3: a) Z-component waveform examples from a southern offshore event located at 34.33°N, 26.05°E at a depth of 20.5 km (depicted by red star in Fig. 2). Data passband filtered between 5 and 20 Hz. Note the marked difference in signal quality

between different OBS stations and the long signal coda at stations LIB1 and LIB3 which is typical for many OBS stations in the south of the study region positioned on top of the thick sedimentary cover of the accretionary complex. Red lines indicate the picked P-onsets. b) Z-component waveform examples from an event within the subducting African slab north of Crete 36.70°N, 26.85°E at a depth of 150 km (indicated by red star in Fig. 2). Data passband filtered between 5 and 20 Hz. Note the high signal to noise ratio for the OBS stations south of Crete indicative of the waveguide qualities of the subducting African slab.

Fig. 4: a) Initial velocity model after Meier et al. (2004a), modified according to information from active seismics (Bohnhoff et al., 20001; Brönner, 2003). v_p/v_s ratio is set to 1.78. b) Final minimum 1-D velocity model obtained by VELEST inversion. The large thickness of the first layer is due to the fact that the deepest OBS was 3.6 km below sea level and had to be contained within this layer. v_p/v_s ratio is set to 1.78.

Fig. 5: Results from the VELEST 1-D velocity inversion. a) The 10 v_p-models with the lowest rms misfit (blue) superposed on all starting models. b) Resultant P-velocity models colour-coded according to their rms-misfits. c) v_p/v_s-ratios obtained by solving for independent S-velocity models. d) Plot of station corrections obtained for the minimum 1-D model. Also plotted are the epicentres of the 435 events used for the initial inversion run.

Fig. 6: Cross-section through 3-D velocity model used for the probabilistic earthquake localization with the NonLinLoc code (Lomax, 2000). Location of the profile is that of profile C - D in Fig. 7.

Fig. 7: Mapview of the event locations obtained by using the minimum 1-D velocity model and corresponding station corrections obtained by the VELEST inversion in conjunction with the probabilistic NLLoc Oct-tree localization scheme.

Fig. 8: a) Initial velocity model rms misfit b) Final 1-D minimum velocity model rms misfit. The events are the 435 earthquakes used for the VELEST inversion. c)

Distribution of the largest error ellipsoid half axis for the probabilistic earthquake localization with the simple 3-D model. d) Distribution of the largest error ellipsoid half axis for the probabilistic earthquake localization using the minimum 1-D velocity model with corresponding station corrections in probabilistic earthquake localization mode.

Fig. 9: Results of synthetic test with linear gradient and probabilistic earthquake location methods. Synthetic travel times to eleven stations of the network surrounding the epicenter were calculated for an event at 34.5 °N, 25.75 °E and 30 km depth. Normally distributed random noise with a standard deviation of 0.3 s for P-waves and 0.6 s for S-waves was added to the synthetic times. The plot shows the results for 200 location runs. a) Distribution of depths calculated with the linear gradient approach. Standard deviation 1.53 km b) Distribution of depths calculated with the probabilistic location method. Standard deviation 1.25 km

Fig. 10: Cross-sections showing the hypocentre distribution along profile AB as obtained by the different localization approaches. a) Initial event localization using a velocity model from literature and a gradient method for event localization b) Minimum 1-D velocity model and corresponding station corrections using the gradient method for event localization c) 3- D velocity model and probabilistic event localization d) Minimum 1-D velocity model and corresponding station corrections using the probabilistic event localization. The width of the selected area for projection is 15 km towards both sides of the profile indicated in Fig. 7.

Fig. 11: Cross-sections showing the hypocentre distribution along profile CD as obtained by the different localization approaches. Same model order as in Fig. 10.

Fig. 12: Example of error ellipsoids calculated with the minimum 1-D velocity model and the probabilistic localization scheme of NonLinLoc. Plotted are all events with an rms misfit of less than 0.5 s, a maximum error ellipsoid half axis of no more than 10 km and a magnitude larger than M_L2.0 in the time interval 10/03/04 until 15/04/04.

Fig. 13: Activity in central and eastern Crete and the adjacent offshore region. Colour depth coding is the same as in Fig. 7. Upper left inset shows the projection of microseismicity on a vertical plane along profile AA'. Events are taken from a maximum distance of 20 km from both sides of the profile.

Fig. 14: a) Magnitude over time plot for all located events during the five recording periods (red stars). Discontinuity of the dataset is caused by recovery and redeployment of the OBS stations. Blue bars at the bottom indicate the number of events per day. b) Magnitude completeness map of the study region produced using the zmap software package (Wiemer, 2001) showing the increase in completeness magnitude with increasing distance from the island of Crete. White regions indicate areas with insufficient data for the calculation of the completeness magnitude. c) Calculated b-values for the LIBNET dataset in the study region. d) Calculated a-values for the LIBNET dataset in the study region.

Fig. 15: Localization of seismogenic zones of the Hellenic forearc south of central and eastern Crete. Structural interpretation is for cross-section C-D in Fig. 7 and superimposed circles depict the microseismicity according to Fig. 11d. Ptolemy and Pliny trenches are indicated as sinistral transtensional structures while the nature of the Strabo trench is still not finally resolved. Upward pointing arrow on Crete indicates the rapid uplift of the island possibly caused by the return flow of metamorphic rocks above the slab.

7 Figures

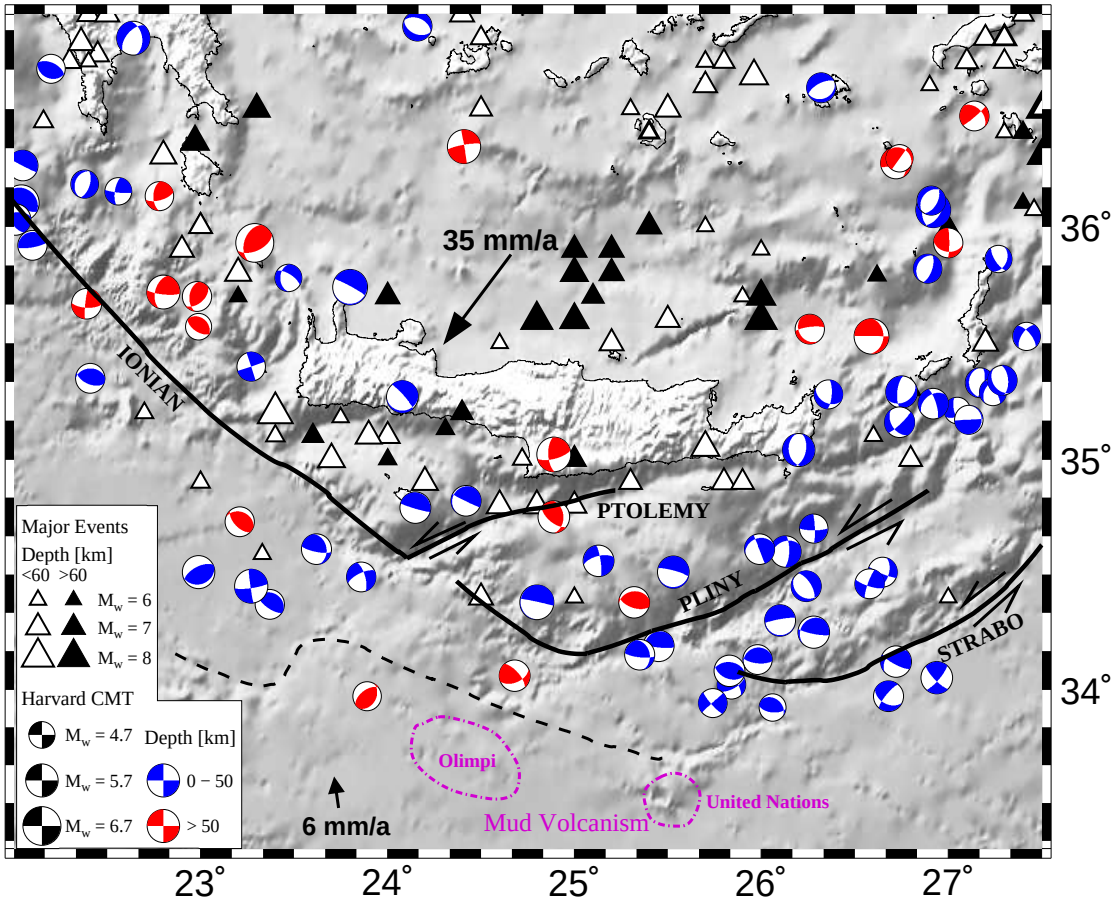

Figure 1: Historic seismicity and Harvard CMT solutions calculated for the convergent plate boundary of the Hellenic Subduction Zone. Major seismicity (black and white triangles) with magnitudes $M_w \geq 6.0$ spans the time period 550 BC - 1999 AD (Papazachos et al., 2000) while beach balls represent fault plane solutions for events between 1977 and 2008 (www.globalcmt.org). Solid black lines indicate the locations of the Ionian, Ptolemy, Pliny and Strabo trenches as seen in the bathymetry and arrows indicate sense of displacement of the transtensional structures (e.g. Kahle et al., 2000; tenVeen and Kleinspehn, 2003). Broken black line indicates the presumed crustal ocean- continent transition. Mud volcano fields in the accretionary prism south of the Pliny and Strabo trenches are indicated by broken magenta lines (Galindo-Zaldivar et al., 1996; Cifci et al., 1997). Plate velocities and directions of movement of the African and Aegean plate are indicated by arrows. Velocities are relative to a stable Eurasian reference frame. See McClusky et al. (2000) for details.

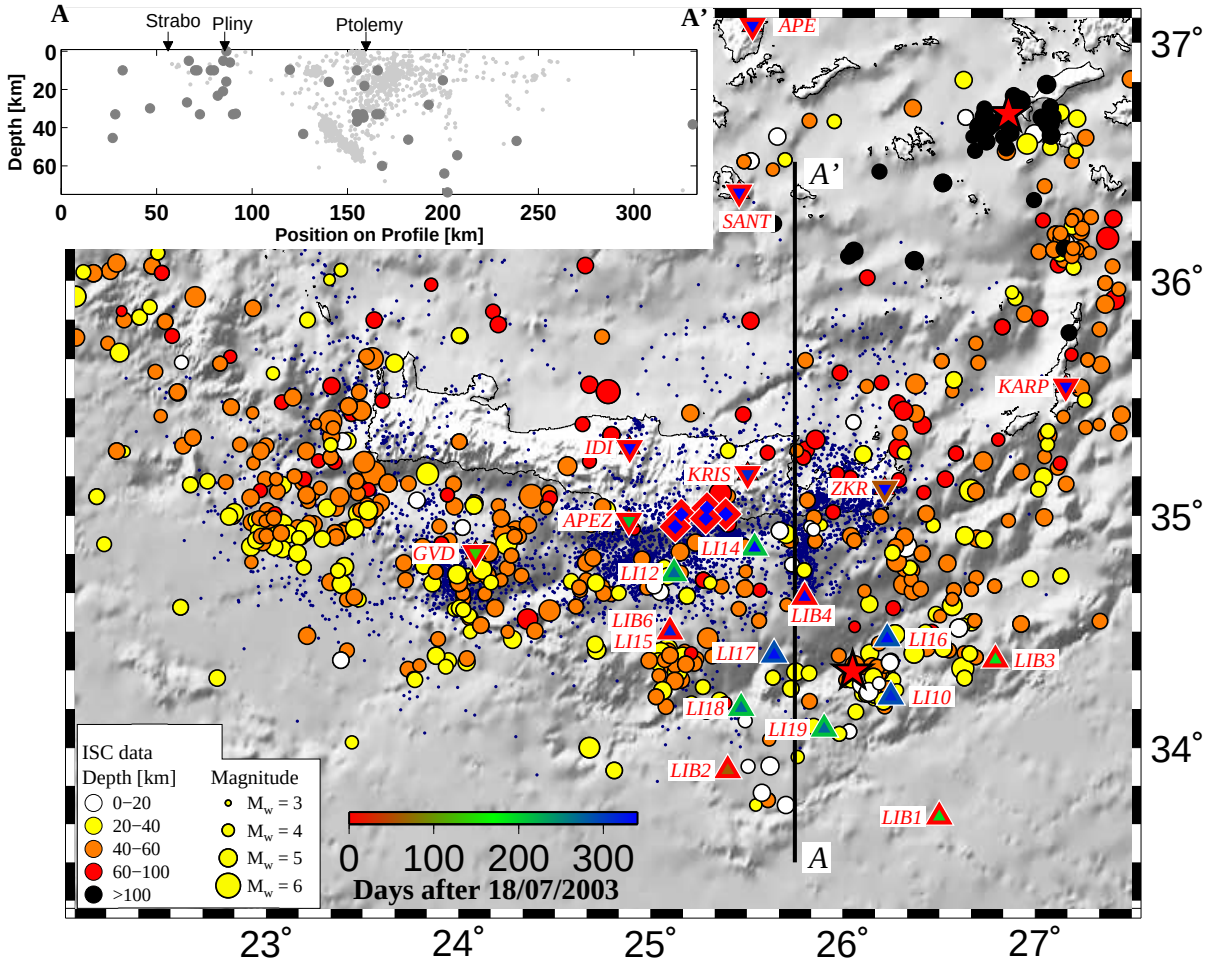

Figure 2: Relocated seismicity according to the ISC catalogue during the time period 1963-1999 (Engdahl et al., 1998) for the region around Crete (circles) and microseismicity located by temporary onshore networks (Meier et al., 2004a; Becker, 2000; blue dots). The configuration of the amphibian seismic network evaluated in this study is superimposed. Triangles mark the OBS locations of LIBNET, diamonds mark temporary short period onshore stations and inverted triangles mark permanent broad-band stations from the GEOFON-, NOA- and MEDNET-networks. Colour-coding of the symbol outline indicates begin of recording while the colour in the symbols interior indicates the end of recording for the respective station. Corresponding colour-scale is given in the lower part of the Figure. Inset: Hypocentres of ISC catalogue events (dark gray dots; Engdahl et al., 1998) and microseismicity recorded with a network on eastern Crete (light gray dots; Becker, 2000) projected on a plane along profile AA'. Events with a distance of up to 20 km from the profile are used for the projection.

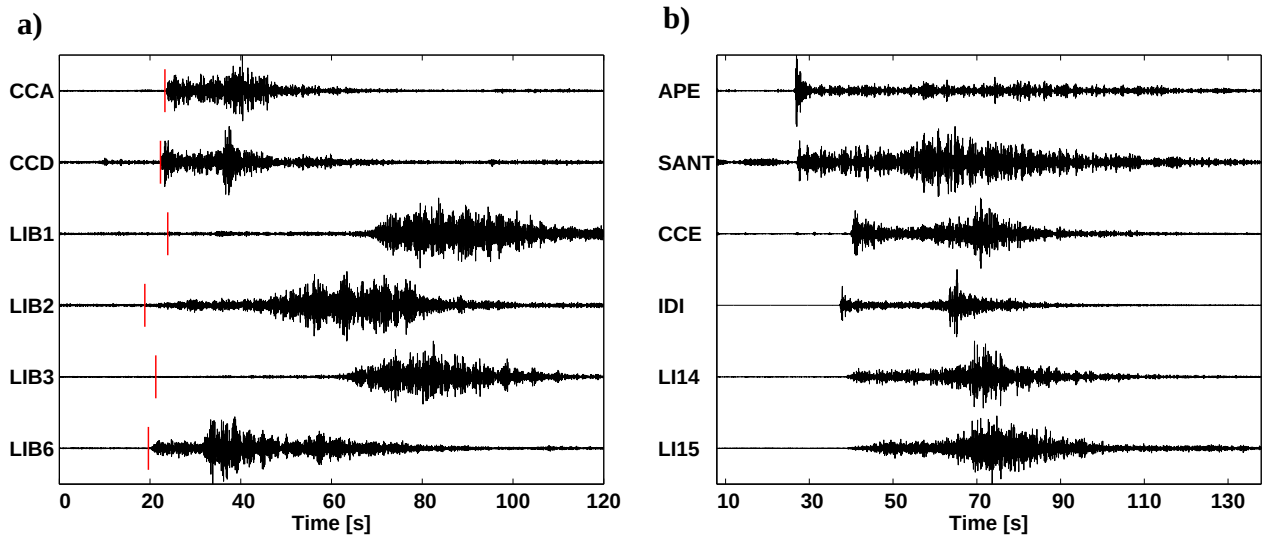

Figure 3: a) Z-component waveform examples from a southern offshore event located at 34.33°N, 26.05°E at a depth of 20.5 km (depicted by red star in Fig. 2). Data passband filtered between 5 and 20 Hz. Note the marked difference in signal quality between different OBS stations and the long signal coda at stations LIB1 and LIB3 which is typical for many OBS stations in the south of the study region positioned on top of the thick sedimentary cover of the accretionary complex. Red lines indicate the picked P-onsets. b) Z-component waveform examples from an event within the subducting African slab north of Crete 36.70°N, 26.85°E at a depth of 150 km (indicated by red star in Fig. 2). Data passband filtered between 5 and 20 Hz. Note the high signal to noise ratio for the OBS stations south of Crete indicative of the waveguide qualities of the subducting African slab.

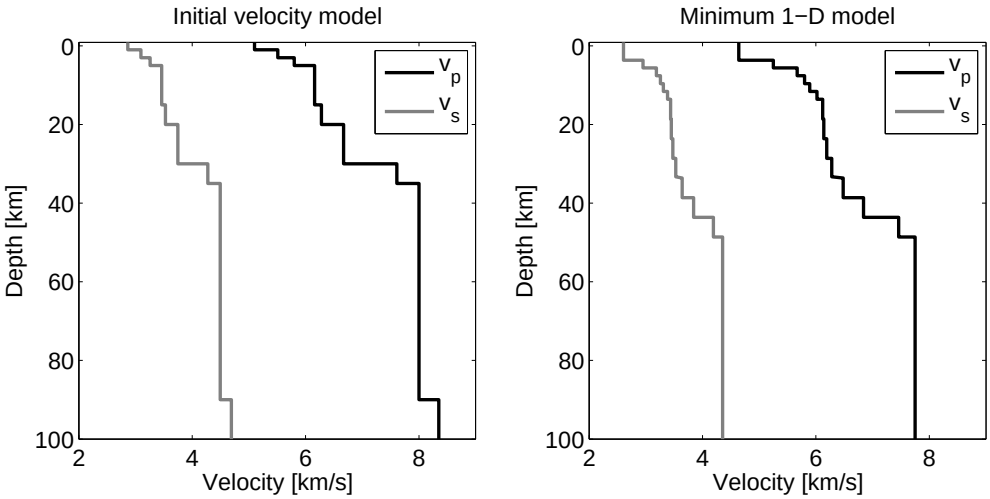

Figure 4: a) Initial velocity model after Meier et al. (2004a), modified according to information from active seismics (Bohnhoff et al., 20001; Brönner, 2003). v_p/v_s ratio is set to 1.78. b) Final minimum 1-D velocity model obtained by VELEST inversion. The large thickness of the first layer is due to the fact that the deepest OBS was 3.6 km below sea level and had to be contained within this layer. v_p/v_s ratio is set to 1.78.

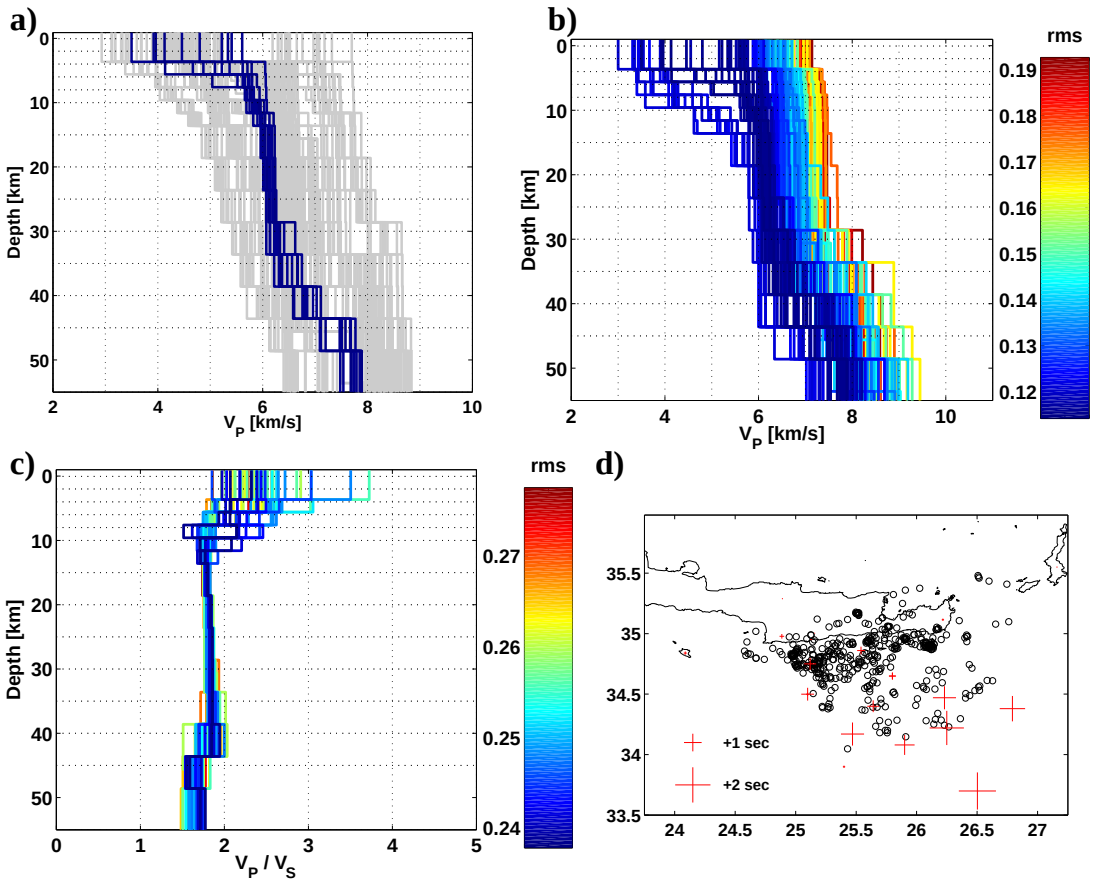

Figure 5: Results from the VELEST 1-D velocity inversion. a) The 10 v_p-models with the lowest rms misfit (blue) superposed on all starting models. b) Resultant P-velocity models colour-coded according to their rms-misfits. c) v_p/v_s-ratios obtained by solving for independent S-velocity models. d) Plot of station corrections obtained for the minimum 1-D model. Also plotted are the epicentres of the 435 events used for the initial inversion run.

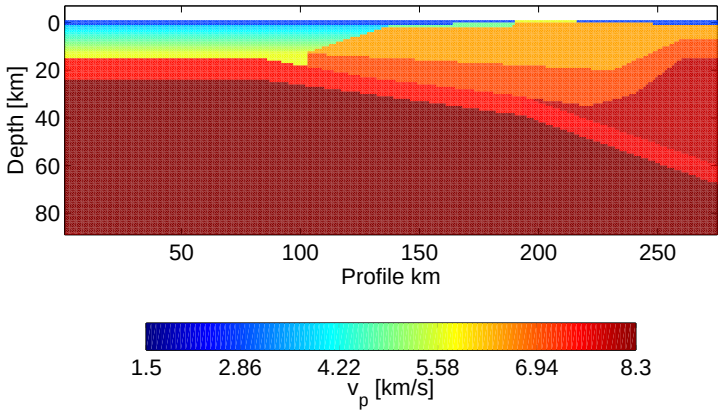

Figure 6: Cross-section through 3-D velocity model used for the probabilistic earthquake localization with the NonLinLoc code (Lomax, 2000). Location of the profile is that of profile C - D in Fig. 7.

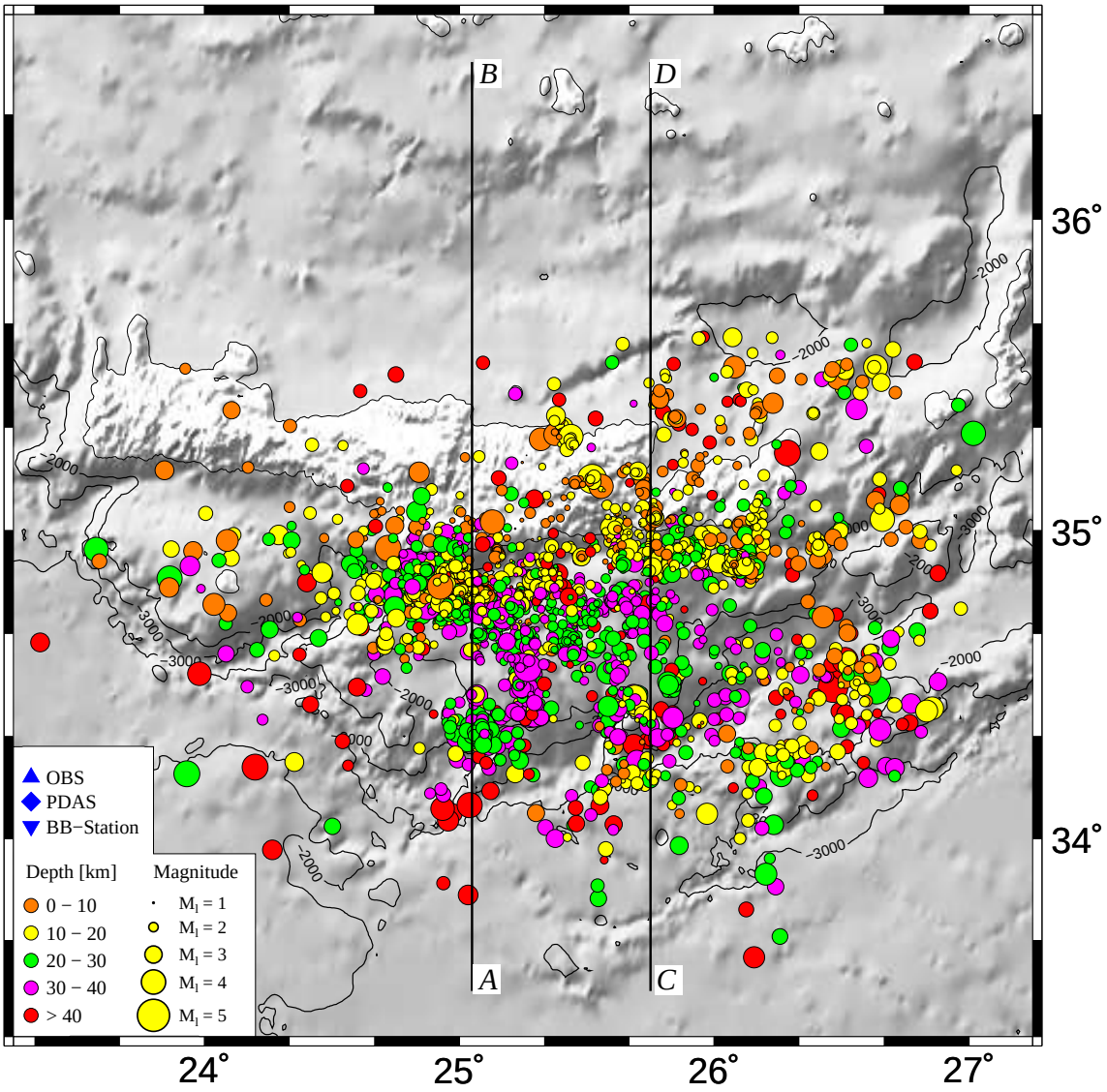

Figure 7: Mapview of the event locations obtained by using the minimum 1-D velocity model and corresponding station corrections obtained by the VELEST inversion in conjunction with the probabilistic NLLoc Oct-tree localization scheme.

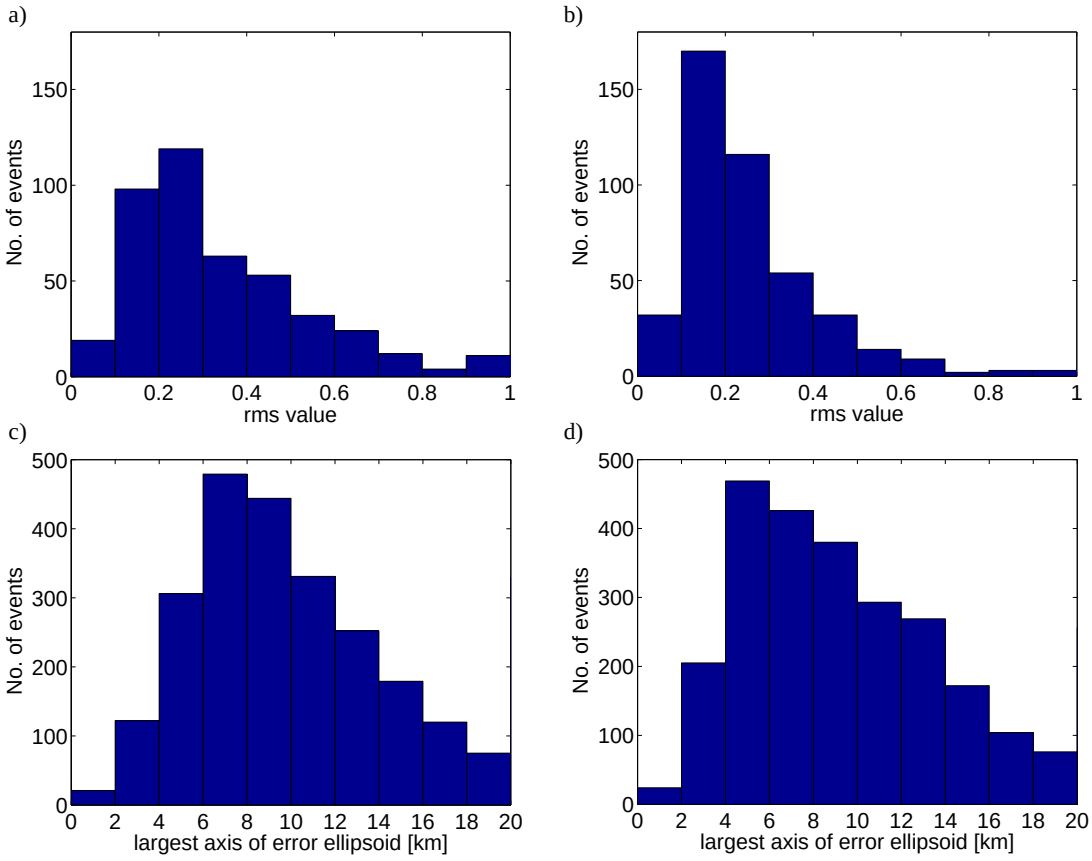

Figure 8: a) Initial velocity model rms misfit b) Final 1-D minimum velocity model rms misfit. The events are the 435 earthquakes used for the VELEST inversion. c) Distribution of the largest error ellipsoid half axis for the probabilistic earthquake localization with the simple 3-D model. d) Distribution of the largest error ellipsoid half axis for the probabilistic earthquake localization using the minimum 1-D velocity model with corresponding station corrections in probabilistic earthquake localization mode.

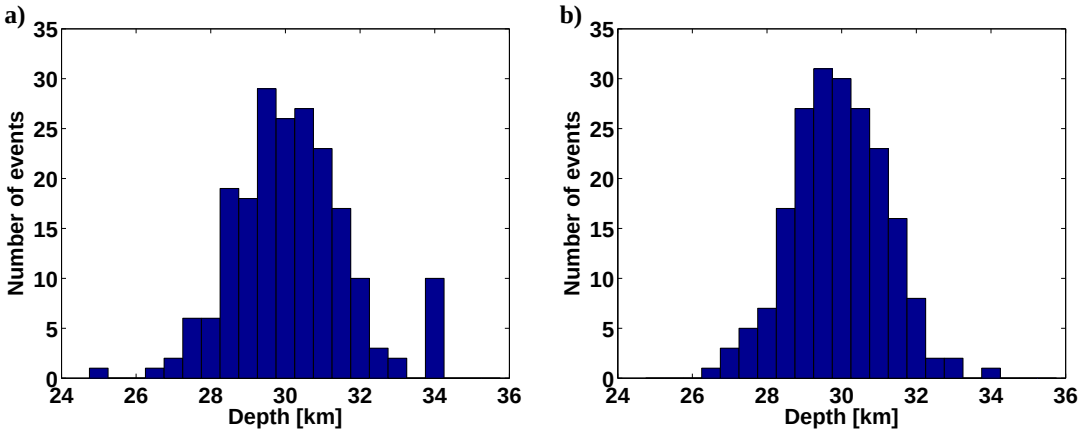

Figure 9: Results of synthetic test with linear gradient and probabilistic earthquake location methods. Synthetic travel times to eleven stations of the network surrounding the epicenter were calculated for an event at 34.5 °N, 25.75 °E and 30 km depth. Normally distributed random noise with a standard deviation of 0.3 s for P-waves and 0.6 s for S-waves was added to the synthetic times. The plot shows the results for 200 location runs. a) Distribution of depths calculated with the linear gradient approach. Standard deviation 1.53 km b) Distribution of depths calculated with the probabilistic location method. Standard deviation 1.25 km

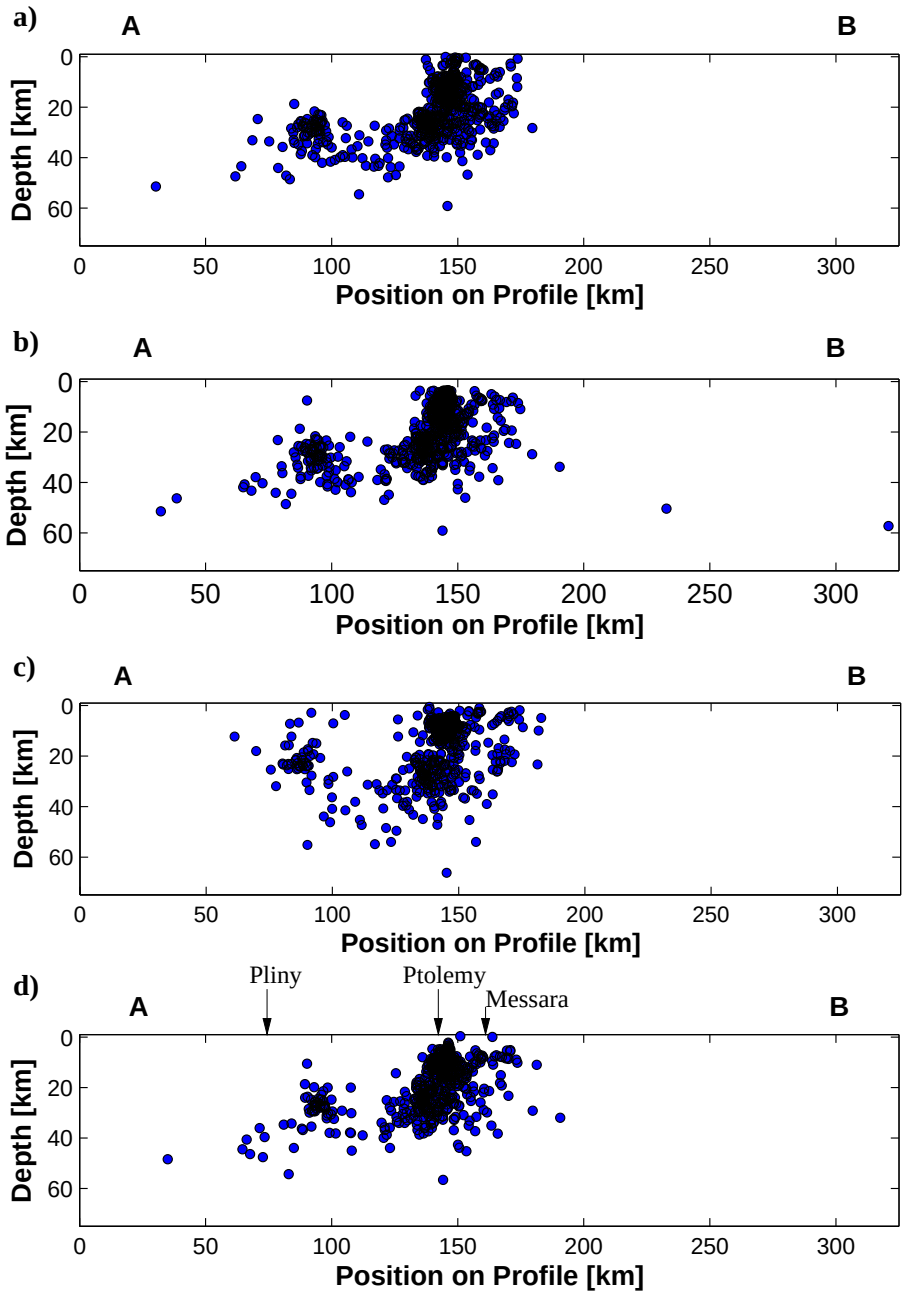

Figure 10: Cross-sections showing the hypocentre distribution along profile AB as obtained by the different localization approaches. a) Initial event localization using a velocity model from literature and a gradient method for event localization b) Minimum 1-D velocity model and corresponding station corrections using the gradient method for event localization c) 3- D velocity model and probabilistic event localization d) Minimum 1-D velocity model and corresponding station corrections using the probabilistic event localization. The width of the selected area for projection is 15 km towards both sides of the profile indicated in Fig. 7.

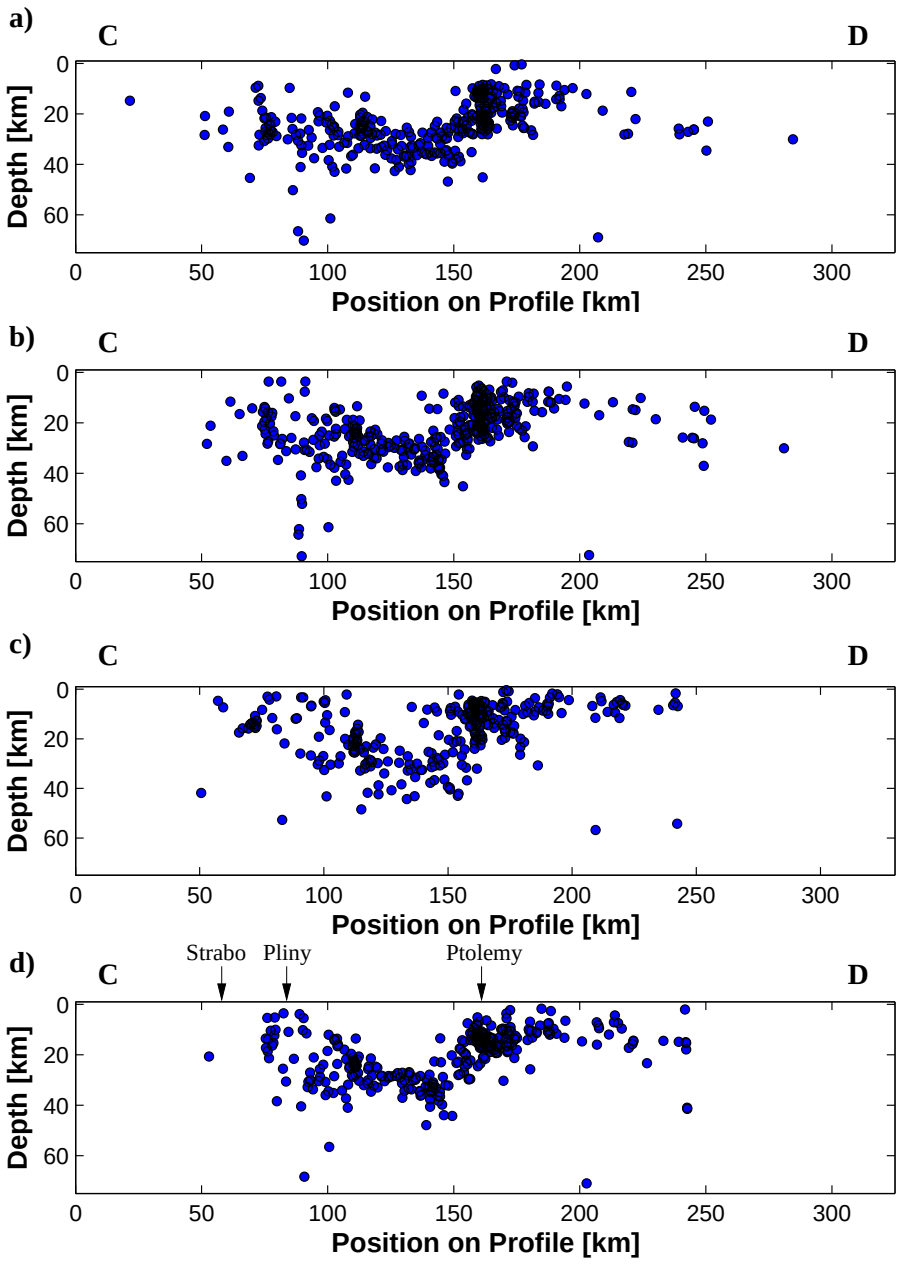

Figure 11: Cross-sections showing the hypocentre distribution along profile CD as obtained by the different localization approaches. Same model order as in Fig. 10.

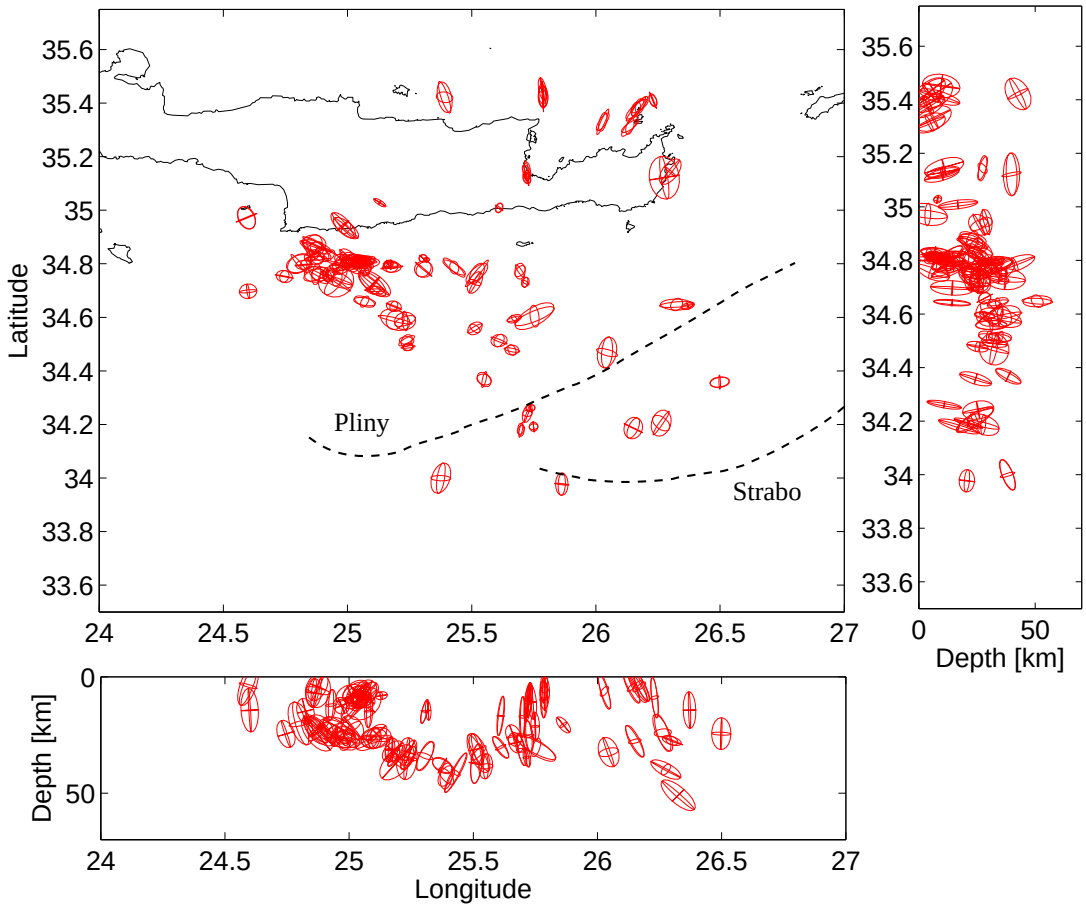

Figure 12: Example of error ellipsoids calculated with the minimum 1-D velocity model and the probabilistic localization scheme of NonLinLoc. Plotted are all events with an rms misfit of less than 0.5 s, a maximum error ellipsoid half axis of no more than 10 km and a magnitude larger than M_L2.0 in the time interval 10/03/04 until 15/04/04.

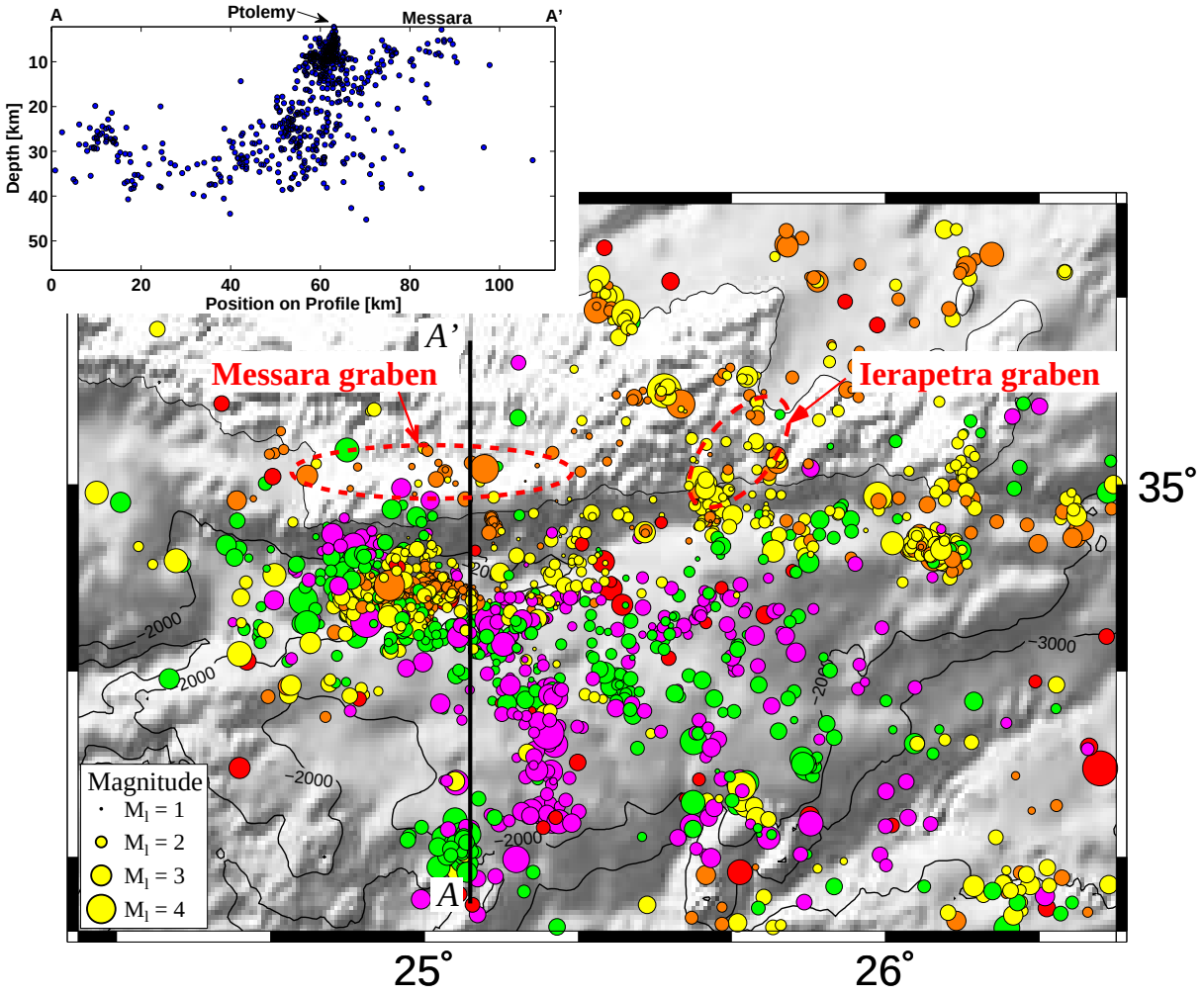

Figure 13: Activity in central and eastern Crete and the adjacent offshore region. Colour depth coding is the same as in Fig. 7. Upper left inset shows the projection of micro-seismicity on a vertical plane along profile AA'. Events are taken from a maximum distance of 20 km from both sides of the profile.

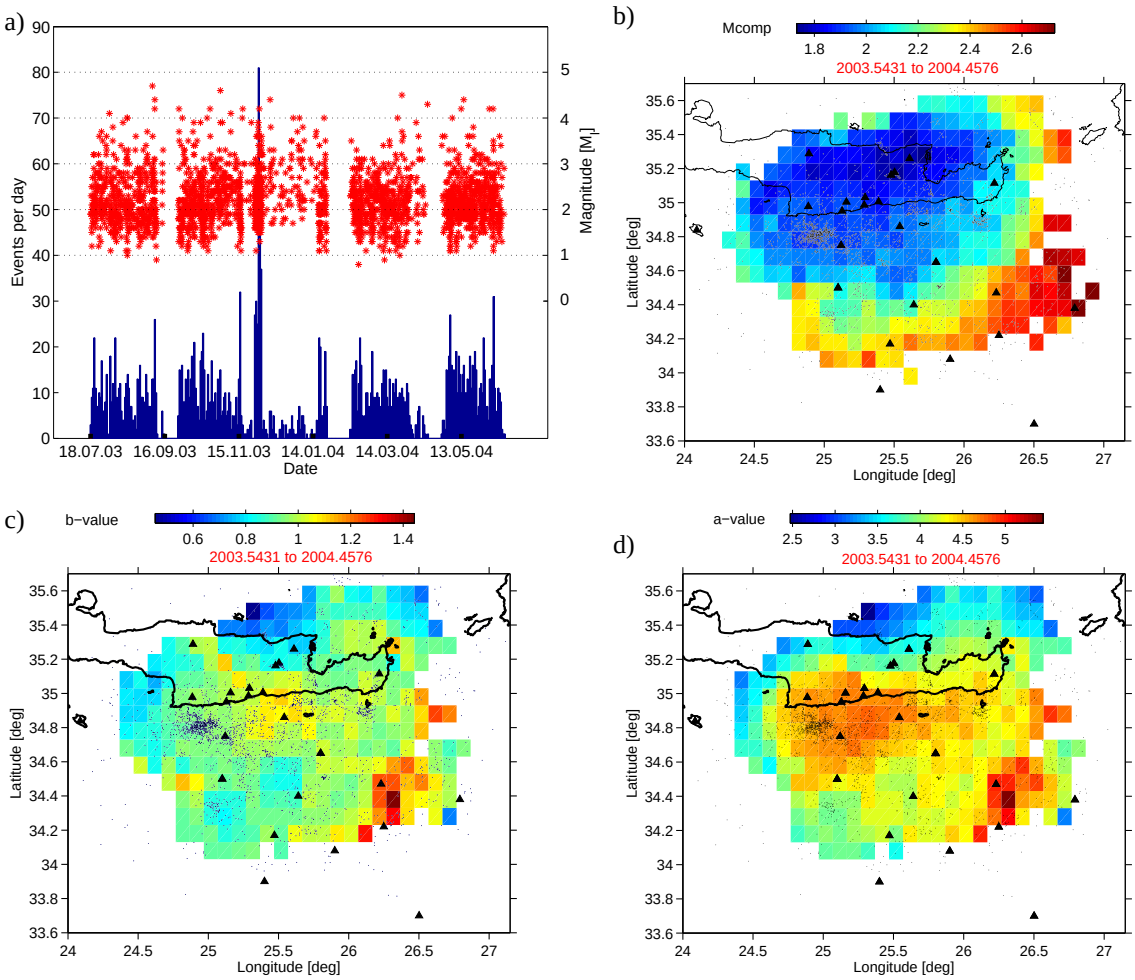

Figure 14: a) Magnitude over time plot for all located events during the five recording periods (red stars). Discontinuity of the dataset is caused by recovery and redeployment of the OBS stations. Blue bars at the bottom indicate the number of events per day. b) Magnitude completeness map of the study region produced using the zmap software package (Wiemer, 2001) showing the increase in completeness magnitude with increasing distance from the island of Crete. White regions indicate areas with insufficient data for the calculation of the completeness magnitude. c) Calculated b- values for the LIBNET dataset in the study region. d) Calculated a-values for the LIBNET dataset in the study region.

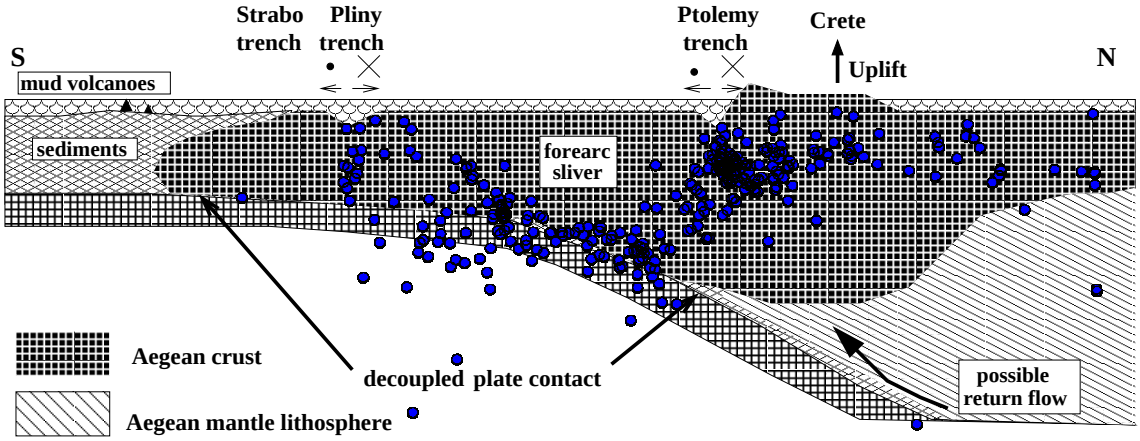

Figure 15: Localization of seismogenic zones of the Hellenic forearc south of central and eastern Crete. Structural interpretation is for cross-section C-D in Fig. 7 and superimposed circles depict the microseismicity according to Fig. 11d. Ptolemy and Pliny trenches are indicated as sinistral transtensional structures while the nature of the Strabo trench is still not finally resolved. Upward pointing arrow on Crete indicates the rapid uplift of the island possibly caused by the return flow of metamorphic rocks above the slab.